Supplementary Information (SI) for ChemComm.
This journal is © The Royal Society of Chemistry 2024

Supporting Information
for

A Stable Radical within a N-Co-N Core

Anirban Bhandari,[†a] Gyeong Min Park,[†a] Heui Beom Lee,[a] Sugyeong Hong,[b] Sun Hee Kim,[b] Hye Ryung Byon,[c] and Yunho Lee[a]*

† A.B. and G.M.P. contributed equally.

[a]Department of Chemistry, Seoul National University, Seoul 08826, Republic of Korea
[b]Western Seoul Centre, Korea Basic Science Institute, Seoul 03759, Republic of Korea
[c]Department of Chemistry, Korea Advanced Institute of Science and Technology (KAIST), Daejeon 34141, Republic of Korea
yunhochem@snu.ac.kr

Contents

Experimental Section.....S4
Figure S1. ^{1}H NMR spectrum of **A** S7
Figure S2. ^{13}C{^{1}H} NMR spectrum of **A** S7
Figure S3. ^{1}H NMR spectrum of **B** S8
Figure S4. ^{13}C{^{1}H} NMR spectrum of **B** S8
Figure S5. ^{31}P NMR spectrum of **B**.....S8
Figure S6. ^{1}H NMR spectrum of **1b**.....S9
Figure S7. ^{1}H NMR spectrum of **2** S10
Figure S8. ^{13}C{^{1}H} NMR spectrum of **2**.....S10
Figure S9. ^{31}P{^{1}H} NMR spectrum of **2**.....S10
Figure S10. The ^{1}H NMR Spectral changes during the reaction of **1b** with NaOH/HCl.....S11
Figure S11. HR-MS spectrum of **A** S12
Figure S12. HR-MS spectrum of **B** S12
Figure S13. ESI-MS spectrum of **1b**.....S13
Figure S14. ESI-MS spectrum of **2**.....S13
Figure S15. HR-MS spectrum of **1b**.....S14
Figure S16. HR-MS spectrum of **2**.....S14
Figure S17. Solid state molecular structure of **1a**.....S15
Table S1. Selected bond distances and angles for **1a**.....S15
Figure S18. Solid state molecular structure of **1b**.....S17
Table S2. Selected bond distances and angles for **1b**.....S17
Figure S19. Solid state molecular structure of **2**.....S18
Table S3. Selected bond distances and angles for **2**.....S18
Table S4. Selected bond distances and angles for **1a**, **1b** and **2**.....S19
Figure S20. Space-filling model of **1b**.....S20
Table S5. Structural comparison of **1** with other reported examples.....S20
Figure S21. UV-Vis spectrum of **1b**.....S21
Figure S22. UV-Vis spectrum of **2**.....S21
Figure S23. UV-Vis spectral changes of **1b** with addition of NaOH.....S22
Figure S24. UV-Vis spectral change of **1b** with addition of cobaltocene.....S22
Figure S25. UV-Vis spectral titration of **1b** with addition of cobaltocene.....S23
Figure S26. UV-Vis spectral titration of **1b** with addition of NaO^{t}Bu.....S23
Figure S27. UV-Vis spectral change of **2** with addition of ferrocenium tetrafluoroborate.....S24
Figure S28. UV-Vis spectral change of **2** with reaction with air and $NaPF_6$.....S24
Figure S29. UV-Vis spectral change of **2** with reaction with air.....S25
Figure S30. UV-Vis spectral change of **2** with reaction with hydrogen peroxide and $NaPF_6$.....S25
Figure S31. UV-Vis spectral change of **2** with reaction with hydrogen peroxide.....S26
Figure S32. Stability test for **1b** monitored by UV-Vis spectroscopy under air or water conditions...S26
Figure S33. IR spectrum of **A**.....S27
Figure S34. IR spectrum of **B**.....S27
Figure S35. IR spectrum of **1a**.....S27
Figure S36. IR spectrum of **1b**.....S28
Figure S37. IR spectrum of **2**.....S28
Figure S38. EPR spectrum of **1b** at room temperature.....S29
Figure S39. EPR spectrum of **1b** at 4 K. S29
Table S6. Comparison of EPR parameters of selected metal-aminyl complexes.....S30
Figure S40. Cyclic voltammogram of **1b**.....S31
Figure S41. Cyclic voltammogram of **2**.....S31
Figure S42. Selected molecular orbitals of **1** and its electronic structure.....S32

Table S7. Structural parameters of **1** obtained from SC-XRD data and DFT calculation...…….....S32
Figure S43. Calculated molecular orbitals of **1**; alpha spin.....S33
Figure S44. Calculated molecular orbitals of **1**; beta spin.....S34
Figure S45. Mulliken spin density plot for **1**.....S35
Figure S46. Selected molecular orbitals of **2** and its electronic structure…….....S36
Table S8. Structural parameters of **2** obtained from SC-XRD data and DFT calculations...…….....S36
References…….…S37

Experimental Section

General Considerations. All manipulations were carried out using standard Schlenk or glovebox techniques under a N_2 or Ar atmosphere. Solvents were deoxygenated and dried by thoroughly sparging with Ar gas followed by passage through an activated alumina column. Solvents were tested with a standard purple solution of sodium benzophenone ketyl in tetrahydrofuran in order to confirm effective oxygen and moisture removal. All reagents were purchased from commercial vendors and used without further purification unless otherwise stated. Both bis(2-bromo-4-methylphenyl)amine[1] and bis[2-(imidazol-1-yl)-4-methylphenyl]amine[2] were prepared according to literature procedure. Elemental Analyses of cobalt complexes were carried out at Sogang Center for Research Facilities on a Thermo Scientific FLASH 1112 series instrument

X-ray Crystallography. The diffraction data of **1a**, **1b** and **2** were collected on a Bruker SMART 1000. A suitable size and quality of crystal was coated with Paratone-N oil and mounted on a Dual-Thickness MicroLoops LD purchased from MiTeGen. The data were collected with graphite-monochromated MoKα radiation (λ = 0.71073 Å) under a stream of N_2(g) at 100 K. Cell parameters were determined and refined by SMART program. Data reduction was performed using SAINT software. An empirical absorption correction was applied using the SADABS program. The structures were solved by direct methods, and all non-hydrogen atoms were subjected to anisotropic refinement by full-matrix least squares on F^2 by using the SHELXTL/PC package. Hydrogen atoms were placed at their geometrically calculated positions and refined riding on the corresponding carbon atoms with isotropic thermal parameters.

Spectroscopic Measurements. An Agilent 400-MR spectrometer was used to measure ^{1}H and ^{31}P NMR spectra and a Varian Inova-500 spectrometer was used to measure the ^{13}C{^{1}H} NMR spectra. Deuterated solvents were purchased from *Deutero*, degassed, and dried over activated 4-Å molecular sieves prior to use. The chemical shifts for ^{1}H NMR spectra are quoted in parts per million (ppm) and are referenced to residual solvent peaks. The chemical shifts in the ^{13}C{^{1}H} NMR spectra are quoted in parts per million (ppm) and are referenced to internal solvent peaks. The *N* values corresponding to ½ [*J*AX+*J*A'X] are provided when virtual couplings are observed in the ^{13}C{^{1}H} NMR spectra. The chemical shifts for ^{31}P spectra are quoted in parts per million (ppm) and are referenced to external phosphoric acid in D_2O at 0.00 ppm. ^{31}P NMR spectra were decoupled by broad band proton decoupling. The following abbreviations were used to describe peak splitting patterns when appropriate: s = singlet, d = doublet, t = triplet, b = broad singlet, m = multiplet, dd = doublet of doublets, td = triplet of doublets, hpt = heptet, coupling constants, *J*, were reported in hertz unit (Hz). UV-Vis spectra were measured by an Agilent Cary 60 UV-Vis spectrophotometer using a 1 cm two-window quartz spectrophotometer cell sealed with a screw-cap purchased from Hellma Analytics (117.100-QS). Infrared spectra were recorded in KBr pellets by Agilent Cary 630. Frequencies are given in reciprocal centimeters (cm^{-1}) and only selected absorbances were reported.

Computational Details. All initial geometries for the computational models for compound **1** and **2** were obtained from the corresponding X-ray crystal structures. Density Functional Theory (DFT)[3] geometry optimizations and frequency calculations were performed at the B3LYP/Def2-SVP level[4a] of theory using the Gaussian 16 package.[4b,c] Optimized structures were verified by the absence of any imaginary frequency. Single point energy evaluations were done at B3LYP/Def2-TZVPP level including the solvent (acetonitrile) implemented through the CPCM[5] scheme. The Def2-SVP basis set was used for all atoms.

Synthesis of A. This ligand was synthesized according to the literature procedure, which is silightly modified as follows. Bis[2-(imidazol-1-yl)-4-methylphenyl]amine was transferred as a green solid (2.79 g, 8.48 mmol) to a sealed tube and dissolved in 30 mL of acetonitrile, followed by the addition of methyl iodide (4.81 g, 33.9 mmol). After the mixture was heated at 40 °C for 16 h, the volatiles were removed under vacuum. The brown organic residue was washed with ethyl acetate (3 X 20 mL) and diethyl ether (3 X 20 mL) and the resulting product bis[2-(3-methylimidazolium)-4-methylphenyl]amine diiodide (**A**; 4.99 g, 8.11 mmol, 95.7%) was isolated as a yellow solid after drying under vacuum. ^{1}H NMR (400 MHz, CD_3CN) δ 9.03 (s, 2H, NC*H*N), 7.49 (s, 2H, Ar-*H*), 7.45 (s, 2H, Ar-*H*), 7.28 (d, *J* = 8.5 Hz, 2H, Im-*H*), 7.24 (s, 2H, Ar-*H*), 7.05 (d, *J* = 8.2 Hz, 2H, Im-*H*), 6.77 (s, 1H, N-*H*), 3.91 (s, 6H, Im-CH_3), 2.34 (s, 6H, Ar-*H*). ^{13}C{^{1}H} NMR (126 MHz, CD_3CN) δ 137.73 (s), 136.11 (s), 134.86 (s), 133.37 (s), 128.47 (s), 126.95 (s), 125.00 (s), 124.54 (s), 122.62 (s), 37.01(d, *J* = 4.28 Hz, Im-CH_3), 20.32 (d, *J* = 2.52 Hz, Ar-CH_3). HR-MS for $\{(C_{22}H_{24}N_5)\}^+$: Calcd, 358.20; Found, 358.20.

Synthesis of B. To a brown solution of **A** (1.50 g, 2.44 mmol) in 15 mL of acetonitrile, $AgPF_6$ (1.23 g, 4.88 mmol) was added and the reaction mixture was stirred at room temperature for 1 h, revealing a light-yellow colour precipitate was immediately formed. The resulting solution was filtered through Celite, the volatiles were removed under vacuum. The resulting product bis[2-(3-methylimidazolium)-4-methylphenyl]amine bishexafluorophosphate (**B**; 1.10 g, 1.69 mmol, 86.0 %) was isolated as a grey solid after washing with diethyl ether (3 X 20 mL) and drying under vacuum. ^{1}H NMR (400 MHz, CD_3CN) δ 8.55 (s, 2H, NC*H*N), 7.43 (s, 4H, Ar-*H*), 7.27 (d, *J* = 7.5 Hz, 2H, Im-*H*), 7.20 (s, 2H, Ar-*H*), 6.96 (d, *J* = 8.3 Hz, 2H, Im-*H*), 5.80 (s, 1H, N-*H*), 3.85 (s, 6H, Im-CH_3), 2.32 (s, 6H, Ar-CH_3). ^{13}C{^{1}H} NMR (126 MHz, CD_3CN) δ 137.73 (s), 136.11(s), 134.86 (s), 133.37 (s), 128.47 (d, *J* = 5.04 Hz), 126.95 (s), 125.00 (d, *J* = 7.56 Hz), 124.54 (d, *J* = 8.82 Hz), 37.01 (d, *J* = 7.56 Hz, Im-CH_3), 20.32 (d, *J* = 3.78 Hz, Ar-CH_3). ^{31}P NMR (162 MHz, CD_3CN) δ –144.61 (hpt, *J* = 706.8 Hz). HR-MS for $\{(C_{22}H_{24}N_5)\}^+$: Calcd, 358.20; Found, 358.20.

Synthesis of $[Co(CNC)_2](I_3)_2$ (1a). To a slurry of **A** (600 mg, 0.98 mmol) in 30 mL of tetrahydrofuran, $CoCl_2$ (63 mg, 0.49 mmol) was added. After the mixture was cooled down to –78 °C, LiHMDS (3.0 mL, 3.0 mmol) was added. The reaction mixture was slowly warmed and stirred at room temperature for 16 h. The resulting solution was taken out of the glove box and the volatiles were removed by rotary evaporator. The resulting green solid was dissolved in dichloromethane (30 mL) and the green solution was stirred at room temperature for 2 h under air. The resulting blue solution was filtered through Celite, the volatiles were removed under vacuum. The resulting blueish green solid was washed with pentane (2 X 5 mL) and drying under vacuum. X-ray quality crystals were grown from the slow evaporation of a saturated solution of **1a** in acetone.

Synthesis of $[Co(CNC)_2](PF_6)_2$ (1b). To a slurry of **B** (0.400 g, 0.614 mmol) in 20 mL of tetrahydrofuran, $CoBr_2$ (67 mg, 0.31 mmol) was added. After the mixture was cooled to –78 °C, LiHMDS (1.9 mL, 1.0 M in tetrahydrofuran, 1.9 mmol) was added dropwise. The reaction mixture was slowly warmed and stirred at room temperature for 4 h. The mixture was taken out of the glove box and the volatiles were removed by rotary evaporator. The resulting green solid was dissolved in dichloromethane (20 mL) and the mixture was stirred for 2 h under air. The resulting blue solution was filtered through Celite, the volatiles were removed under vacuum. The resulting product $[Co(CNC)_2](PF_6)_2$ (**1b**; 302 mg, 0.275 mmol, 89.6%) was isolated as a blue solid after washing with pentane (3 X 10 mL) and drying under vacuum. ESI-MS for $\{(C_{44}H_{44}N_{10}Co)\}^{2+}$: Calcd, 385.65; Found, 385.65. HR-MS for $\{(C_{44}H_{44}CoN_{10})\}^{2+}$: Calcd, 385.6536; Found, 385.6529. Anal. Calcd for $C_{44}H_{44}N_{10}P_2F_{12}Co$: C, 49.75; H, 4.17; N, 13.19. Found: C, 49.74; H, 4. 26; N, 13.25; μ_{eff}: 1.69 μ_B (CD_3CN, 25 °C, Evans' method). UV−vis [CH_3CN, nm (M^{-1} cm^{-1})]: 860 (820), 640 (2100), 565 (2600), 375 (10500), 336 (12300). Crystals suitable for X-ray diffraction were obtained by diffusion of diethyl ether into a saturated solution of **1b** in acetonitrile at room temperature.

Synthesis of $[Co(CNC)_2](PF_6)$ (2). To a solution of **1b** (0.100 g, 0.091 mmol) in 15 mL tetrahydrofuran, KC_8 (14 mg, 0.10 mmol) was added revealing an immediate colour change from blue to green. The reaction mixture was stirred at room temperature for 1 h. The resulting green solution was filtered through Celite, and the volatiles were removed under vacuum. The resulting product $[Co(CNC)_2](PF_6)$ (**2**; 80 mg, 0.087 mmol, 92%) was isolated as a green solid after washing with pentane (2 X 10 mL) and drying under vacuum. ^{1}H NMR (400 MHz, CD_3CN) δ 7.49 (s, 4H, Ar-*H*), 7.06 (s, 4H, Ar-*H*), 6.97 (d, *J* = 8.4 Hz, 4H, Im-*H*), 6.88 (s, 4H, Ar-*H*), 6.65 (d, *J* = 7.1 Hz, 4H, Im-*H*), 2.68 (s, 12H, Im-C*H*$_3$), 2.20 (s, 12H, Ar-C*H*$_3$). ^{13}C{^{1}H} NMR (126 MHz, CD_3CN) δ 177.77 (s, Co-*C* (carbene)), 143.62 (s), 132.92 (s), 127.43 (s), 127.27 (s), 126.38 (s), 125.37 (s), 120.83 (s), 120.42 (d, *J* = 5.04 Hz), 35.27 (d, *J* = 3.86 Hz, Im-*C*H$_3$), 20.22 (d, *J* = 3.86 Hz, Ar-*C*H$_3$). ^{31}P NMR (162 MHz, CD_3CN) δ –144.62 (hpt, *J* = 706.3 Hz). UV−vis [CH_3CN, nm (M^{-1} cm^{-1})]: 605 (1900), 364 (16100). ESI-MS for $\{(C_{44}H_{44}N_{10}Co)\}^+$: Calcd, 771.31; Found, 771.52. HR-MS for $\{(C_{44}H_{44}CoN_{10})\}^+$: Calcd, 771.3071; Found, 771.3055. Anal. Calcd for $C_{44}H_{44}N_{10}PF_6Co$: C, 57.64; H, 4.83; N, 15.28. Found: C, 57.30; H, 5.11; N, 15.25; X-ray quality crystals were grown by diffusion of pentane into a saturated solution of **2** in dichloromethane at room temperature.

Figure S1. ^{1}H NMR spectrum of **A** in CD_3CN at room temperature.

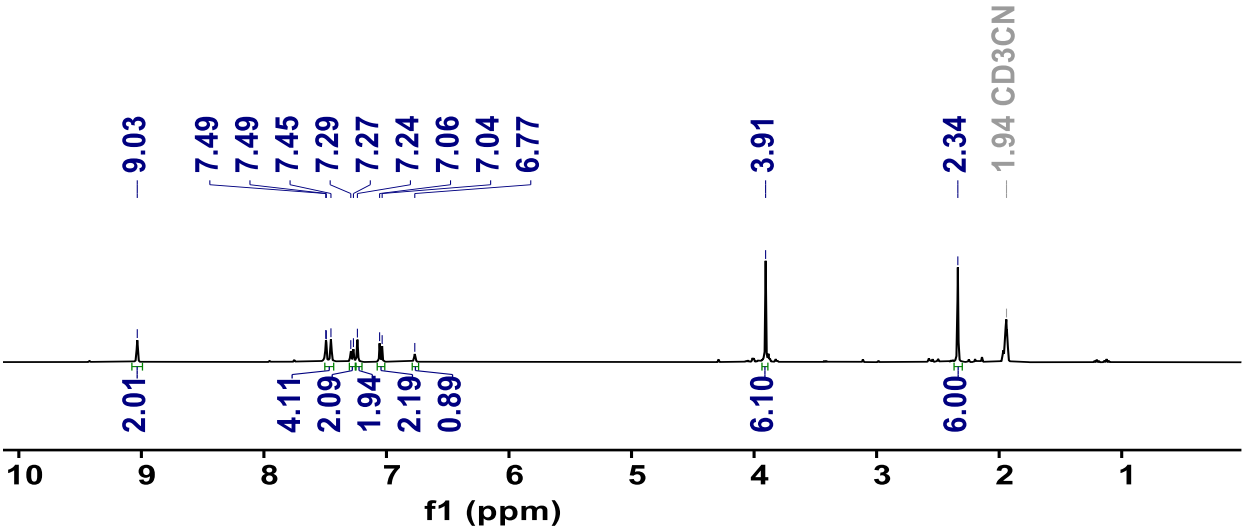

Figure S2. $^{13}C\{^{1}H\}$ NMR spectrum of **A** in CD_3CN at room temperature.

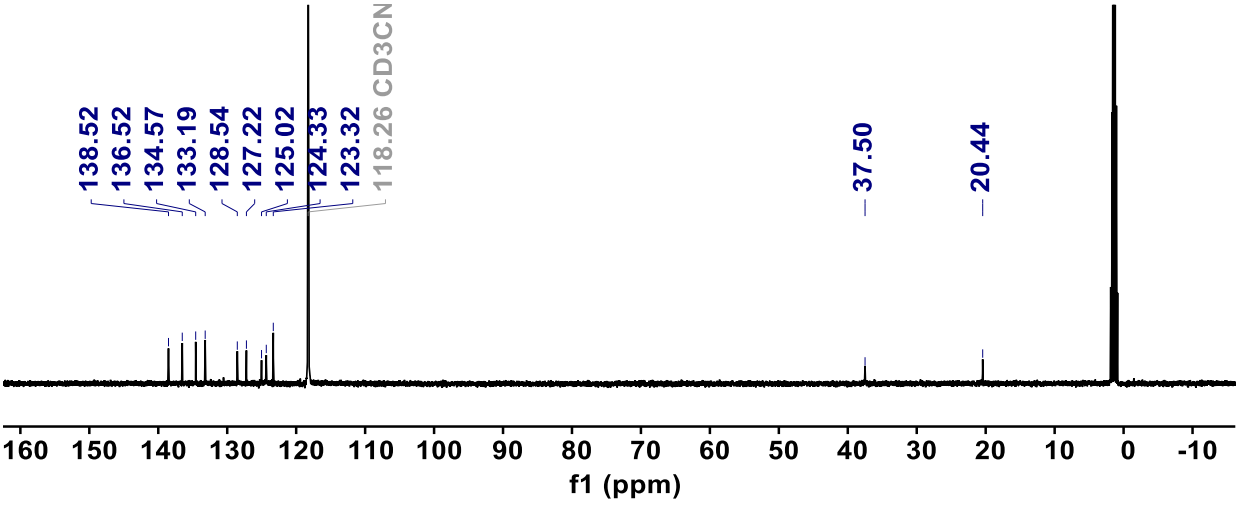

Figure S3. ^{1}H NMR spectrum of **B** in CD_3CN at room temperature.

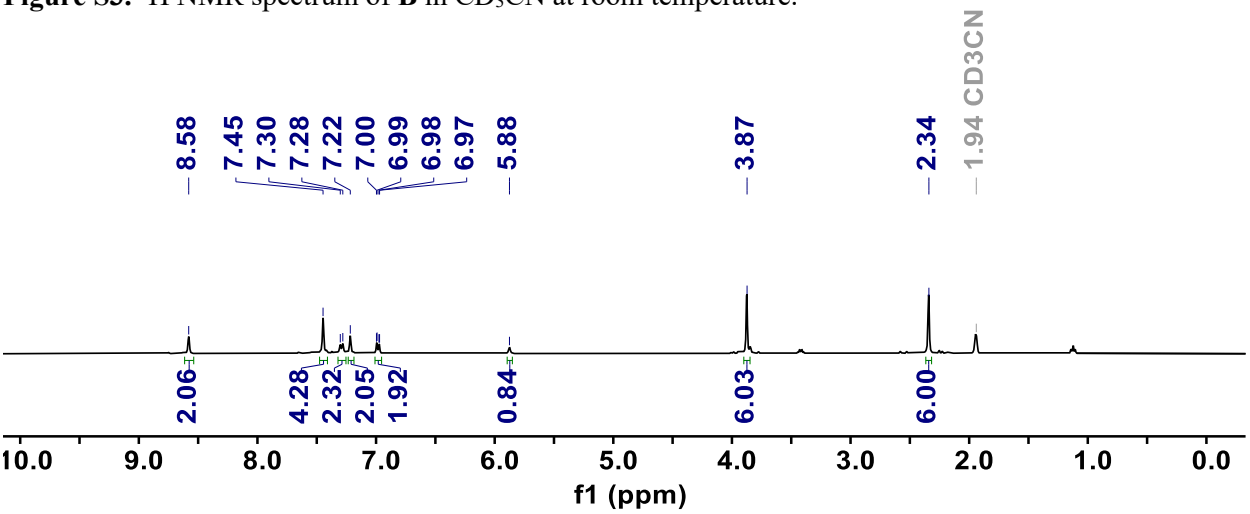

Figure S4. $^{13}C\{^{1}H\}$ NMR spectrum of **B** in CD_3CN at room temperature.

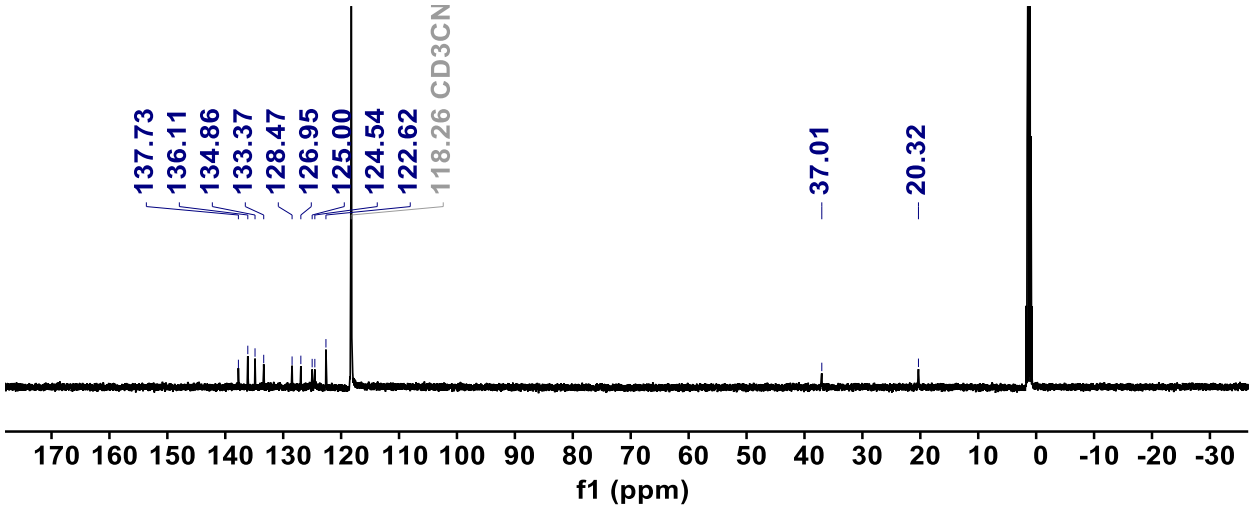

Figure S5. $^{31}P\{^{1}H\}$ NMR spectrum of **B** in CD_3CN at room temperature.

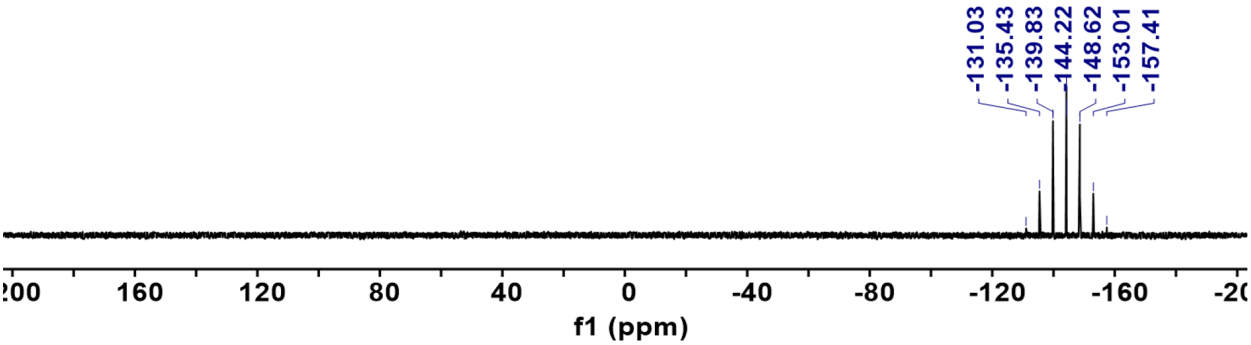

Figure S6. ^{1}H NMR spectrum of **1b** in CD_3CN at room temperature.

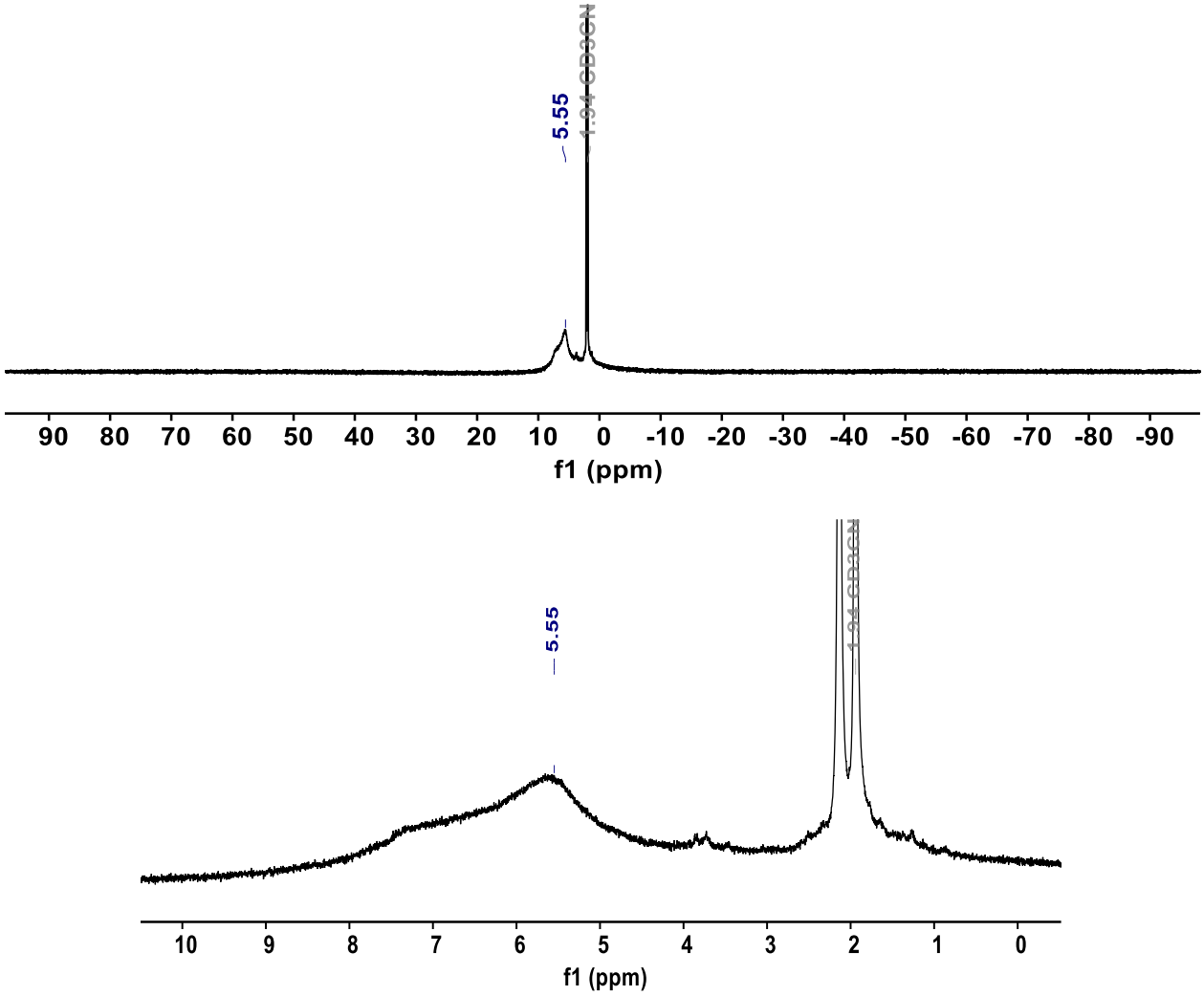

Figure S7. ^{1}H NMR spectrum of **2** in CD_3CN at room temperature.

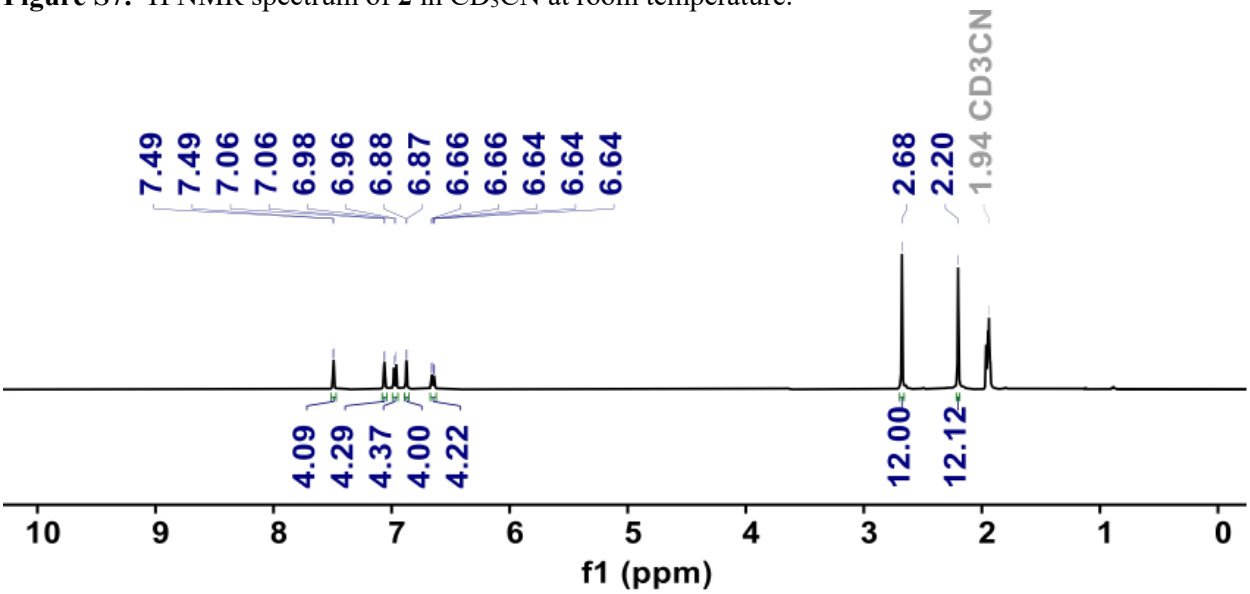

Figure S8. ^{13}C{^{1}H} NMR spectrum of **2** in CD_3CN at room temperature.

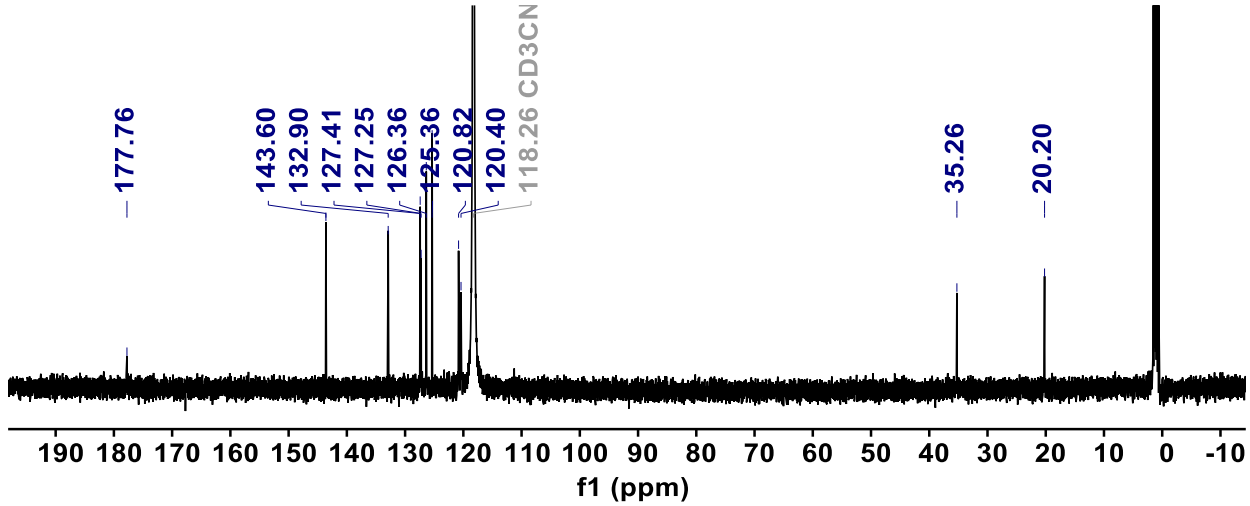

Figure S9. ^{31}P NMR spectrum of **2** in CD_3CN at room temperature.

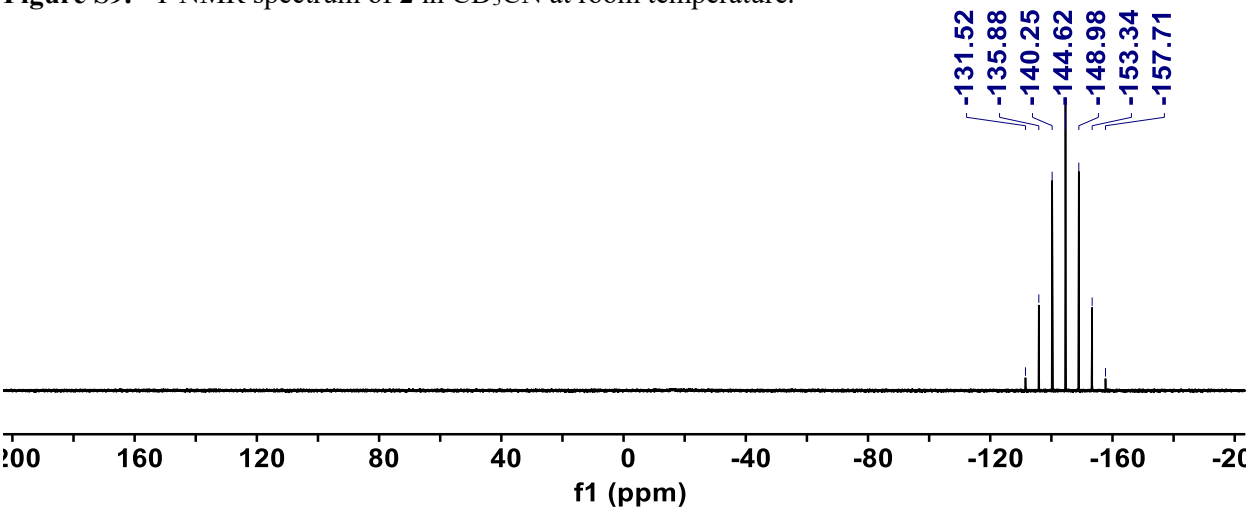

Figure S10. Spectral changes in the ^{1}H NMR spectrum during the reaction of **1b** with NaOH(aq) and HCl(aq) in CD_3CN at room temperature.

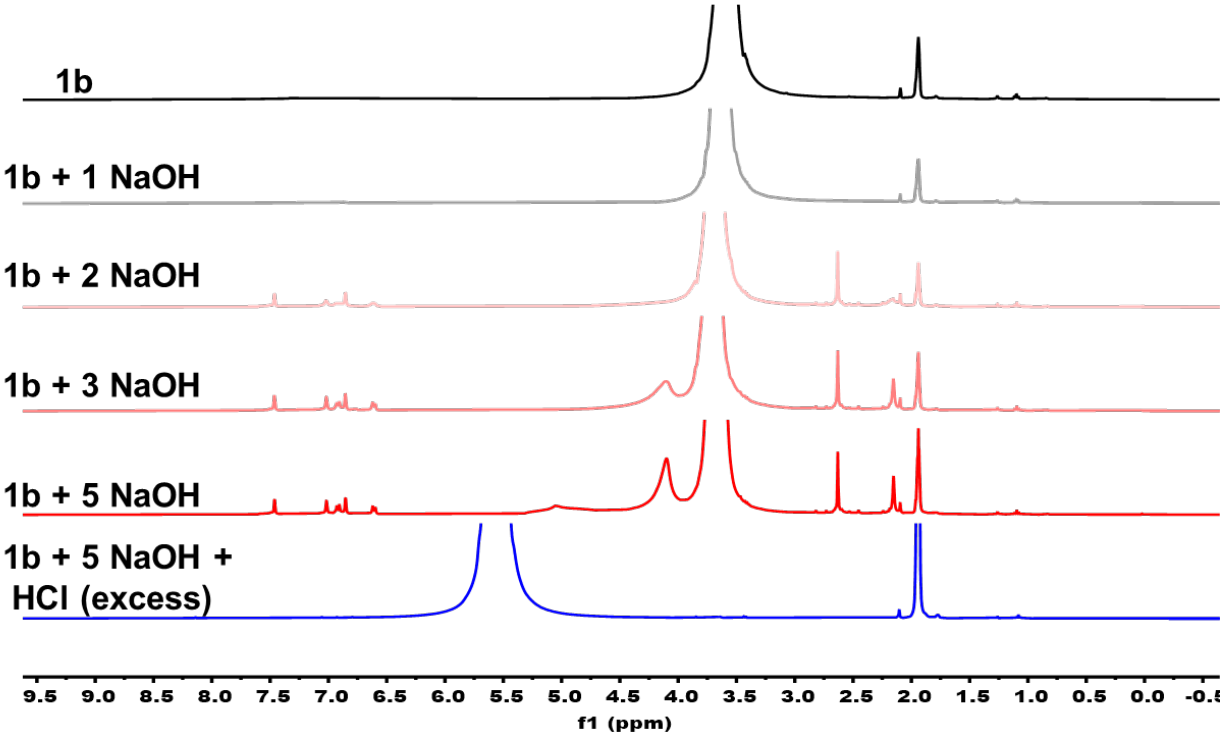

Figure S11. HR-Ms spectrum of **A** at room temperature in CH_3CN.

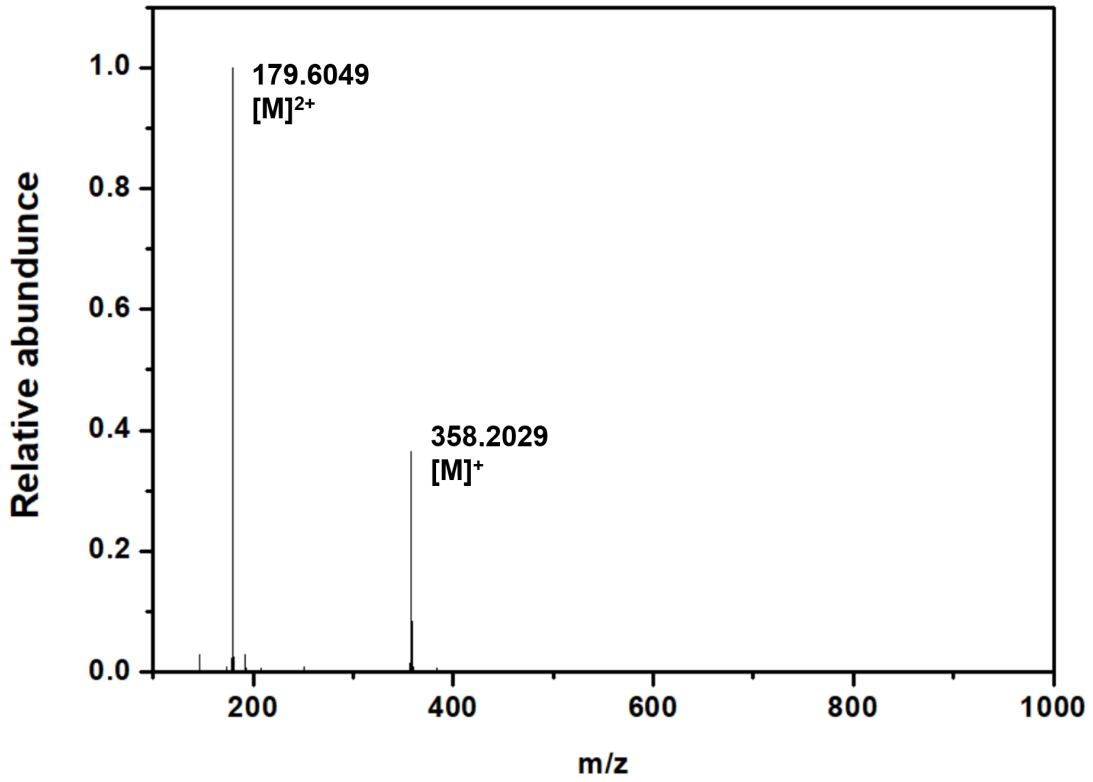

Figure S12. HR-MS spectrum of **B** collected at room temperature in CH_3CN.

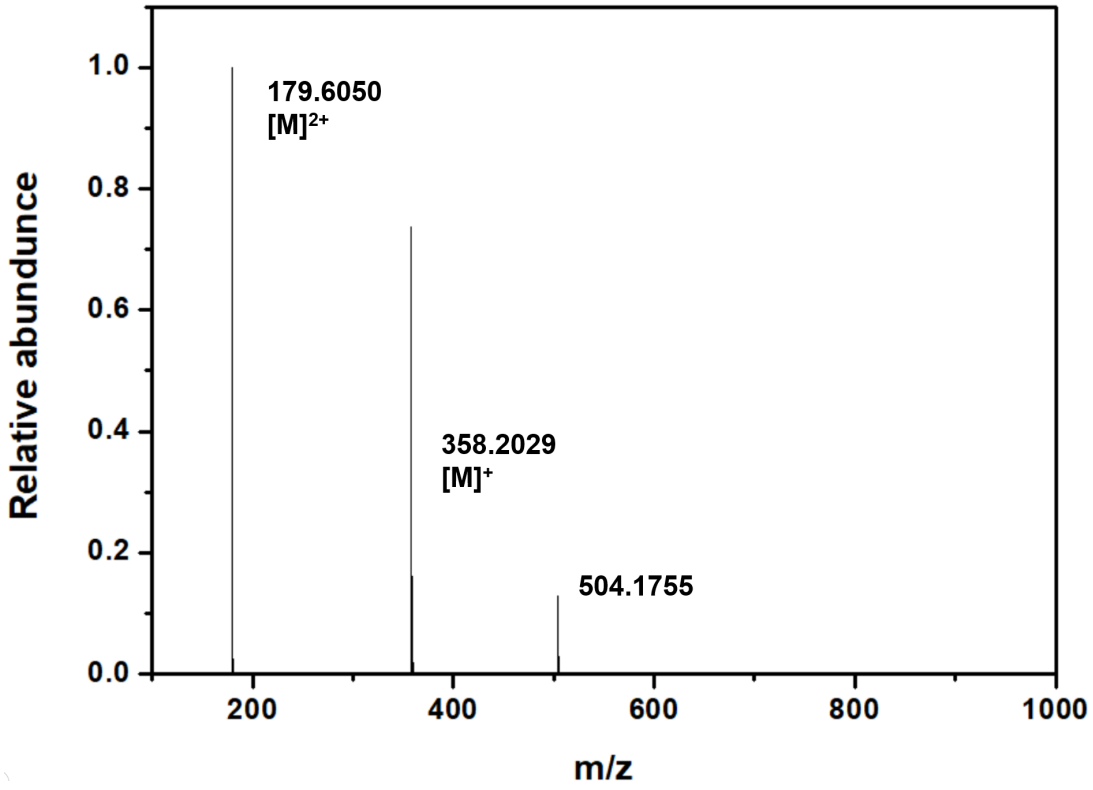

Figure S13. ESI-MS spectrum of **1b** collected at room temperature in CH_3CN. Full scan (left) and expanded region showing the isotope pattern with 0.5 m/z difference (right).

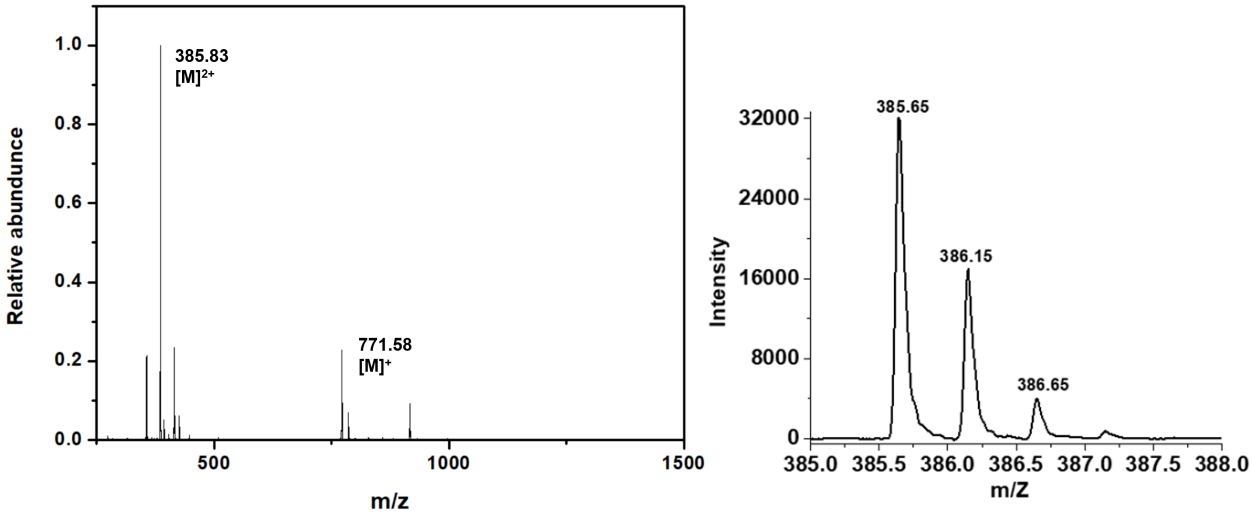

Figure S14. ESI-MS spectrum of **2** collected at room temperature in CH_3CN.

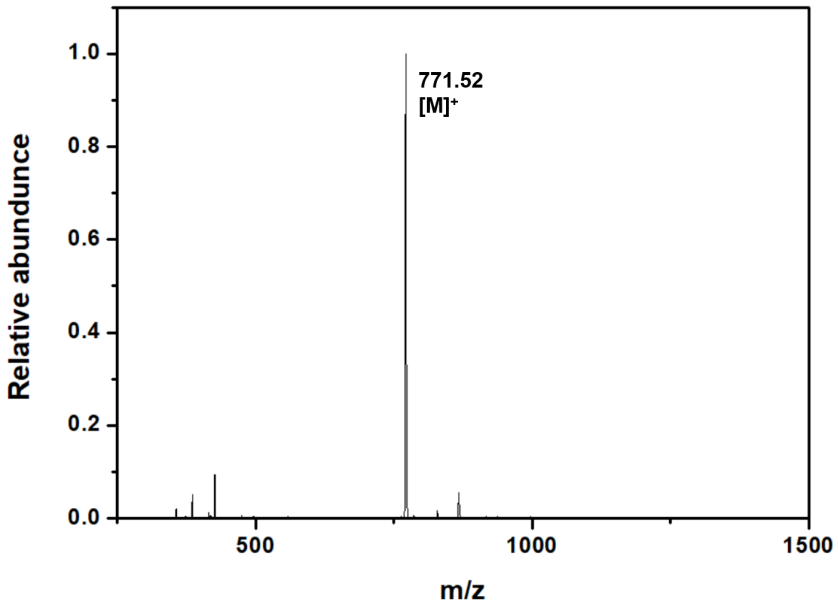

Figure S15. HR-MS spectrum of **1b** collected at room temperature in CH_3CN.

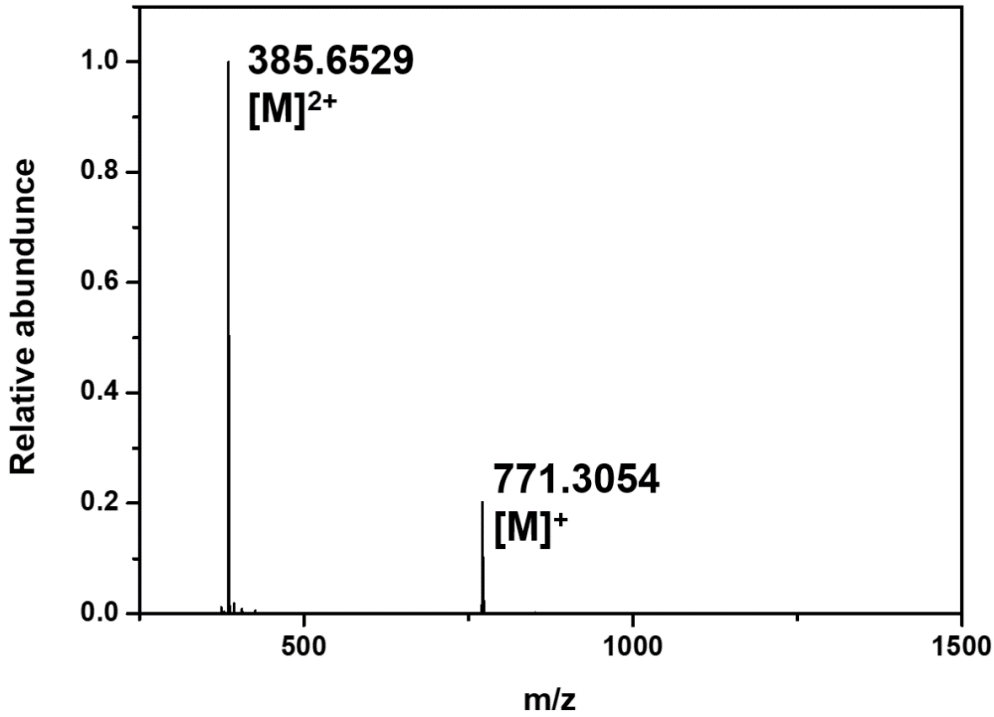

Figure S16. HR-MS spectrum of **2** collected at room temperature in CH_3CN.

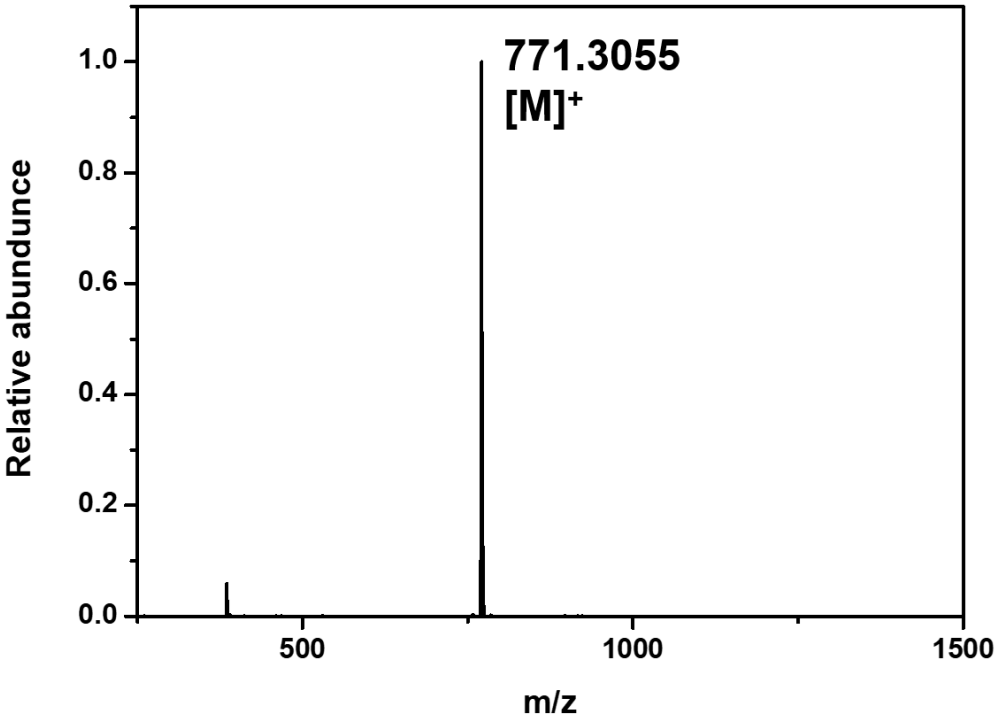

Figure S17. Solid-state structure of **1a**. All hydrogen atoms are omitted for clarity.

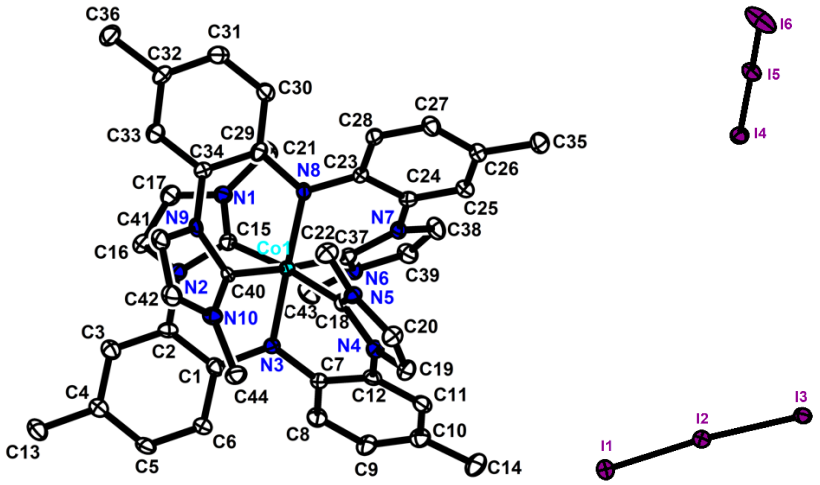

Table S1. Selected bond distances and angles for **1a**.

Bond Distances (Å)		Bond Angles (°)	
$d_{Co1\text{-}N3}$	1.932(4)	∠N3-Co1-N8	178.66(19)
$d_{Co1\text{-}C40}$	1.949(5)	∠N3-Co1-C37	91.51(19)
$d_{Co1\text{-}N8}$	1.922(4)	∠N3-Co1-C15	86.73(18)
$d_{Co1\text{-}C15}$	1.946(6)	∠N3-Co1-C18	87.85(18)
$d_{Co1\text{-}C18}$	1.948(6)	∠N8-Co1-C18	91.71(18)
$d_{Co1\text{-}C37}$	1.946(4)	∠N8-Co1-C37	87.24(19)
$d_{N3\text{-}C7}$	1.407(6)	∠N8-Co1-C40	88.24(19)
$d_{N3\text{-}C1}$	1.390(6)	∠C15-Co1-C18	174.1(2)
$d_{N8\text{-}C23}$	1.389(6)	∠C15-Co1-C37	90.83(18)
$d_{N8\text{-}C29}$	1.392(6)	∠N3-Co1-C40	93.01(19)
		∠Co1-N8-C23	120.4(3)
		∠N8-Co1-C15	93.77(18)
		∠Co1-N8-C29	120.1(3)
		∠C18-Co1-C40	88.0(2)
		∠C34-N9-C40	124.8(4)

	∠C37-Co1-C40	175.5(2)
	∠C34-N9-C41	123.3(4)
	∠C18-Co1-C37	91.77(18)
	∠C40-N9-C41	111.4(4)
	∠C15-Co1-C40	89.9(2)

Figure S18. Solid-state structure of **1b**. A co-crystalized diethyl ether molecule and all hydrogen atoms are omitted for clarity.

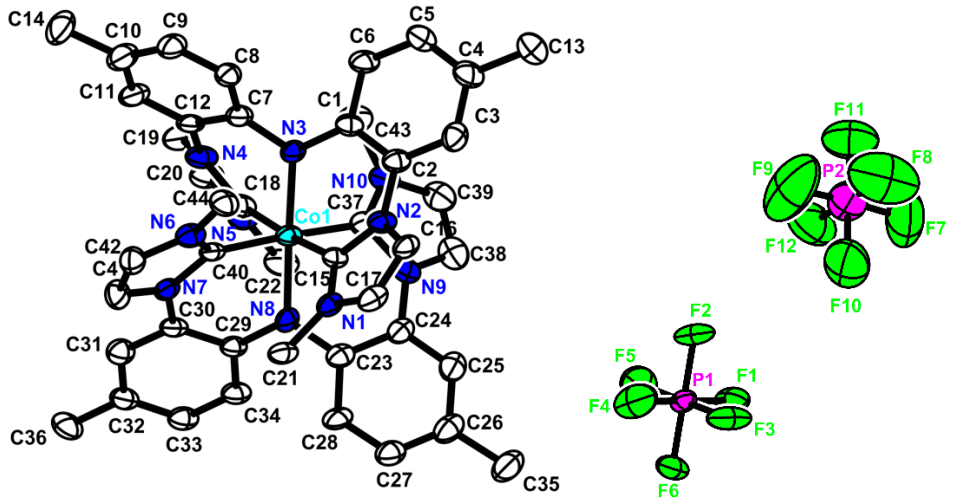

Table S2. Selected bond distances and angles for **1b**.

Bond Distances (Å)		Bond Angles (°)	
$d_{Co1\text{-}N3}$	1.920(4)	∠N3-Co1-N8	177.9(3)
$d_{Co1\text{-}N8}$	1.908(6)	∠N3-Co1-C15	86.6(2)
$d_{Co1\text{-}C15}$	1.949(7)	∠N3-Co1-C18	88.2(2)
$d_{Co1\text{-}C18}$	1.951(7)	∠N3-Co1-C37	91.2(3)
$d_{Co1\text{-}C37}$	1.964(9)	∠N3-Co1-C40	92.7(3)
$d_{Co1\text{-}C40}$	1.949(8)	∠N8-Co1-C15	91.4(3)
$d_{N8\text{-}C29}$	1.386(10)	∠N8-Co1-C18	93.9(3)
$d_{N8\text{-}C23}$	1.389(11)	∠N8-Co1-C37	88.4(3)
$d_{N3\text{-}C1}$	1.399(10)	∠N8-Co1-C40	87.8(3)
$d_{N3\text{-}C7}$	1.396(11)	∠C15-Co1-C18	174.7(3)
		∠C15-Co1-C37	93.7(3)
		∠C15-Co1-C40	88.6(3)
		∠C18-Co1-C37	87.2(3)
		∠C18-Co1-C40	90.9(3)
		∠C37-Co1-C40	175.6(3)

Figure S19. Solid-state structure of **2**. All hydrogen atoms are omitted for clarity.

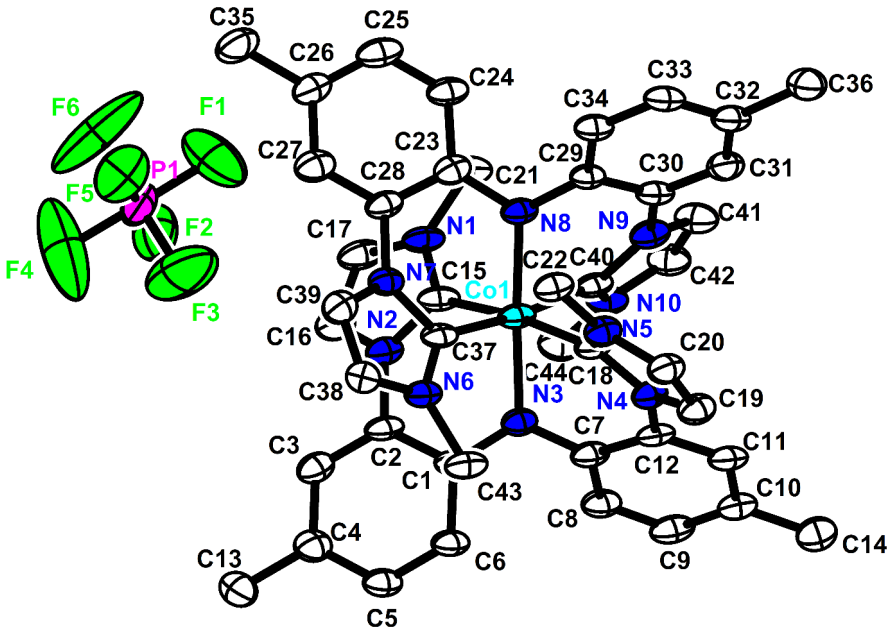

Table S3. Selected bond distances and angles for **2**.

Bond Distances (Å)		Bond Angles (°)	
$d_{Co1\text{-}N3}$	1.973(5)	∠N3-Co1-N8	177.2(2)
$d_{Co1\text{-}N8}$	1.956(5)	∠N3-Co1-C15	86.6(2)
$d_{Co1\text{-}C15}$	1.936(7)	∠N3-Co1-C18	86.7(3)
$d_{Co1\text{-}C18}$	1.934(7)	∠N3-Co1-C37	94.4(2)
$d_{Co1\text{-}C37}$	1.930(6)	∠N3-Co1-C40	91.9(2)
$d_{Co1\text{-}C40}$	1.939(6)	∠N8-Co1-C15	95.3(2)
$d_{Co2\text{-}C84}$	1.938(6)	∠C15-Co1-C18	173.2(3)
$d_{Co2\text{-}N18}$	1.953(5)	∠N8-Co1-C18	91.4(3)
$d_{Co2\text{-}C59}$	1.926(6)	∠N8-Co1-C37	87.7(2)
$d_{Co2\text{-}N13}$	1.964(6)	∠N8-Co1-C40	86.0(2)
$d_{Co2\text{-}C81}$	1.933(6)	∠C15-Co1-C37	90.0(3)
$d_{Co2\text{-}C62}$	1.929(6)	∠C15-Co1-C40	90.1(3)
$d_{N3\text{-}C1}$	1.378(8)	∠C18-Co1-C37	88.8(3)
$d_{N3\text{-}C7}$	1.402(8)	∠C18-Co1-C40	91.9(3)
$d_{N8\text{-}C23}$	1.398(8)	∠C37-Co1-C40	173.7(3)

d_{N8-C29}	1.391(8)	∠N13-Co2-N18	175.6(2)
$d_{N18-C73}$	1.382(8)	∠N13-Co2-C81	91.6(3)
$d_{N18-C67}$	1.399(8)	∠N13-Co2-C84	95.6(3)
$d_{N13-C45}$	1.400(9)	∠N18-Co2-C59	95.5(2)
$d_{N13-C51}$	1.387(8)	∠N18-Co2-C62	90.7(3)
		∠N18-Co2-C81	86.4(3)
		∠N18-Co2-C84	86.7(3)
		∠C59-Co2-C62	173.8(3)
		∠C59-Co2-C81	88.3(3)
		∠C59-Co2-C84	88.8(3)
		∠C62-Co2-C81	91.9(3)
		∠C62-Co2-C84	91.8(3)
		∠C81-Co2-C84	172.2(3)
		∠N13-Co2-C59	88.4(3)
		∠N13-Co2-C62	85.4(3)

Table S4. Selected bond distances (Å) and angles (°) for **1a**, **1b** and **2**.

	d_{Co-C}	d_{Co-N}	∠N–Co–N	∠C–Co–C
1a	1.949(5), 1.946(6) 1.948(6), 1.946(4)	1.932(4) 1.922(4)	178.7(2)	174.1(2) 175.5(2)
1b	1.949(7), 1.951(7) 1.964(9), 1.949(8)	1.919(4) 1.909(6)	177.9(3)	174.7(3) 175.6(3)
2	1.930(6), 1.935(7) 1.936(7), 1.939(6)	1.973(5) 1.939(6)	177.1(2)	173.7(3) 173.2(3)

Figure S20. Space-filling model of **1b**. All of anions are omitted for clarity.

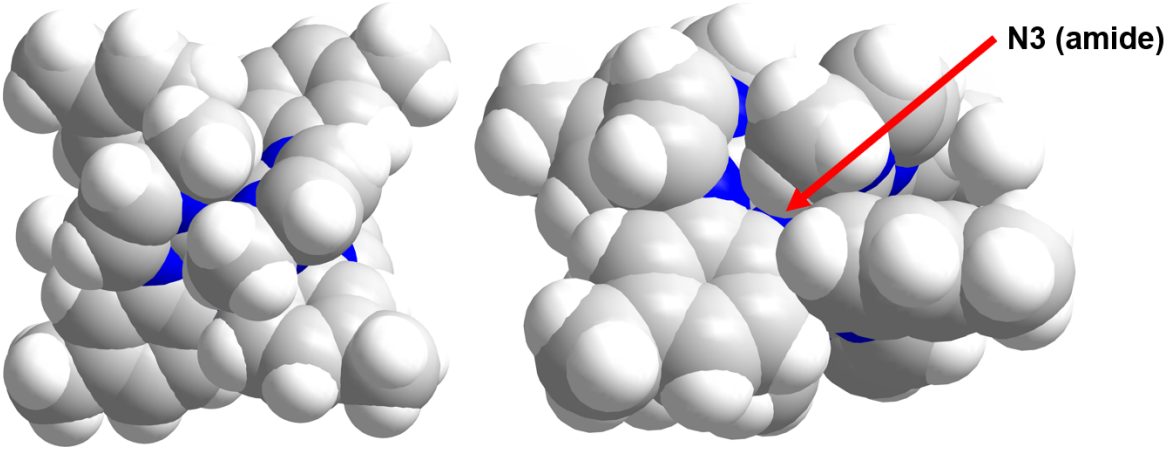

Table S5. Structural comparison of **1** with other reported examples (I, II and III)

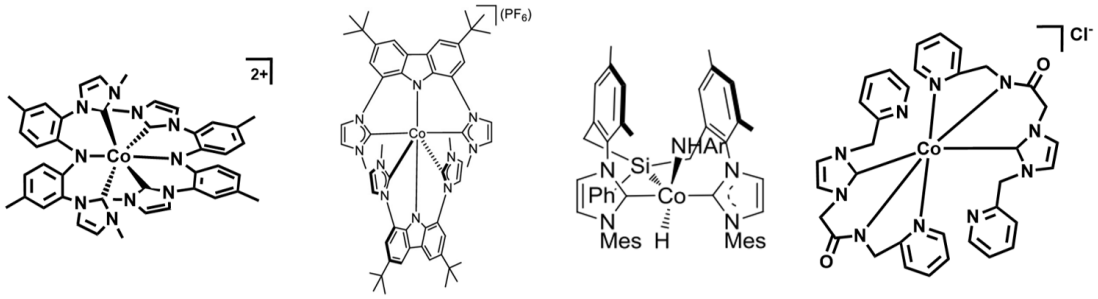

1 I II III

Entry	$d_{Co\text{-}N}$ (Å)	Reference
1	1.920(4), 1.908(6)	This work
I	1.910(2), 1.910(2)	*J. Am. Chem. Soc.* 2022, **144**, 9859–9873
II	1.924(1)	*Angew. Chem. Int. Ed,* 2017, **56**, 2720–2724
III	1.923(5), 1.935(3), 1.911(9)	*Eur. J. Inorg. Chem.*, 2019, **5**, 617–627

Figure S21. UV-Vis spectrum of **1b** in CH_3CN at room temperature.

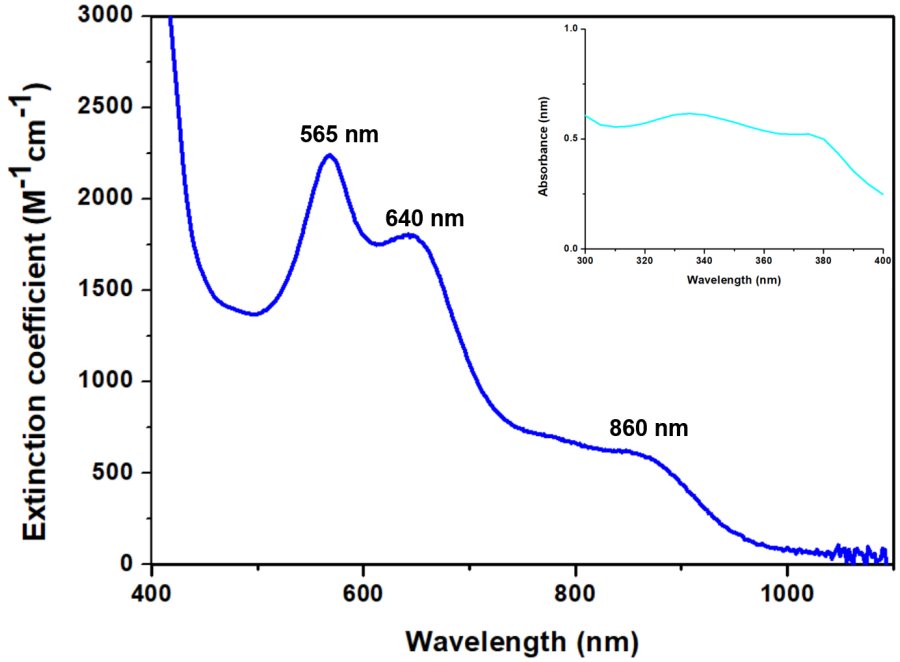

Figure S22. UV-Vis spectrum of **2** in CH_3CN at room temperature.

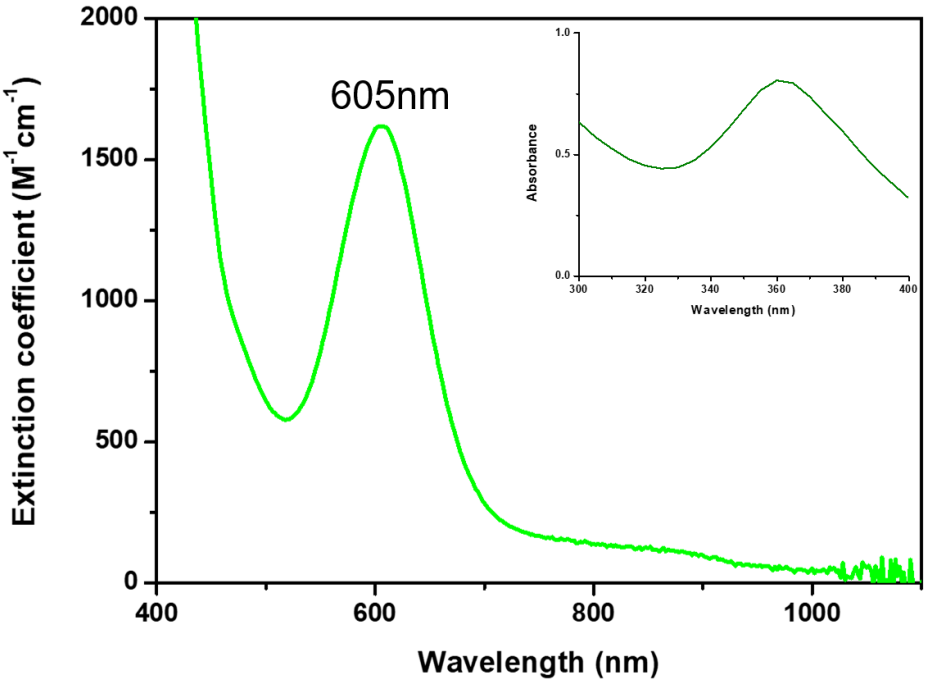

Figure S23. UV-Vis spectral changes upon addition of NaOH (total 180 equivalent; 30 equivalent each time) to **1b** in CH_3CN:H_2O (1:1) at room temperature.

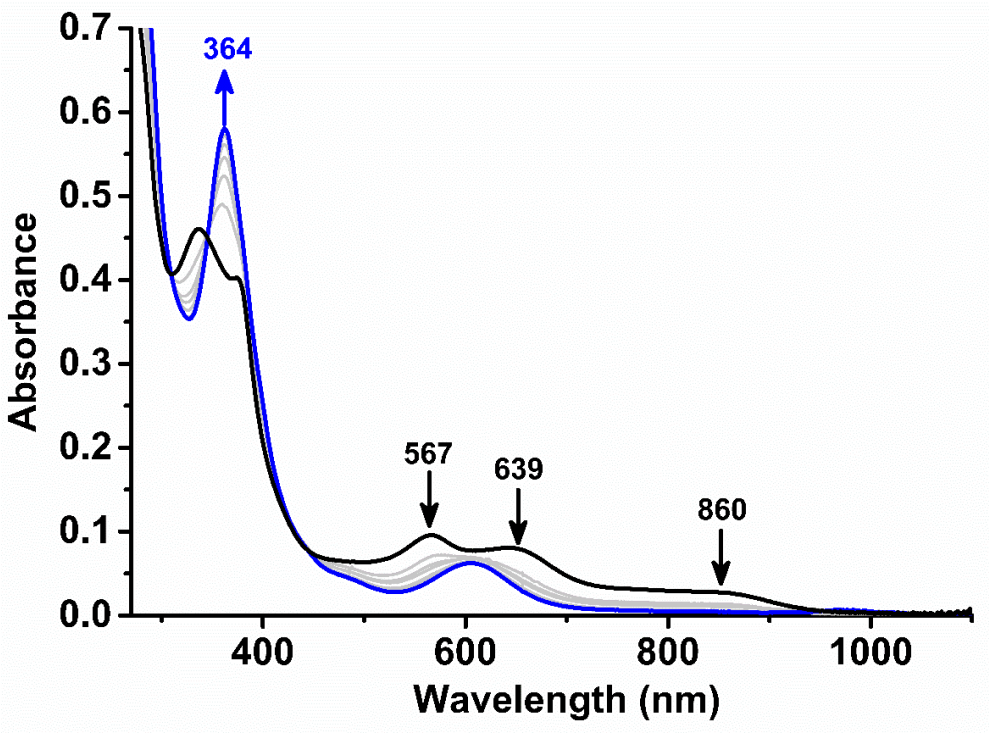

Figure S24. UV-Vis spectral change upon addition of cobaltocene (1 equivalent) to **1b** in CH_3CN at room temperature.

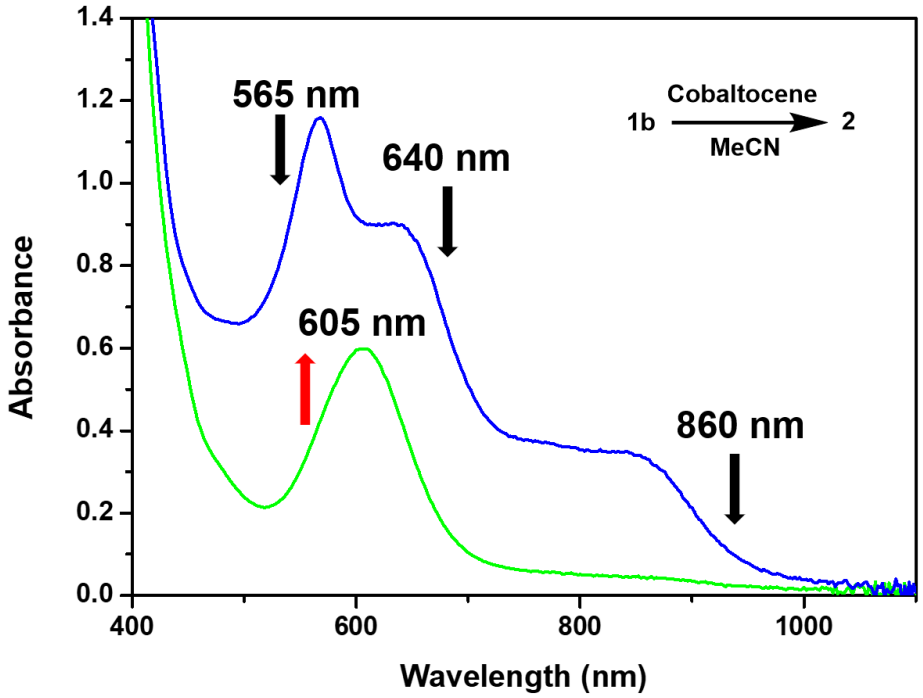

Figure S25. UV-Vis spectral changes upon addition of cobaltocene (total 1 equivalent; 0.2 equivalent each time) to **1b** in CH_3CN at room temperature.

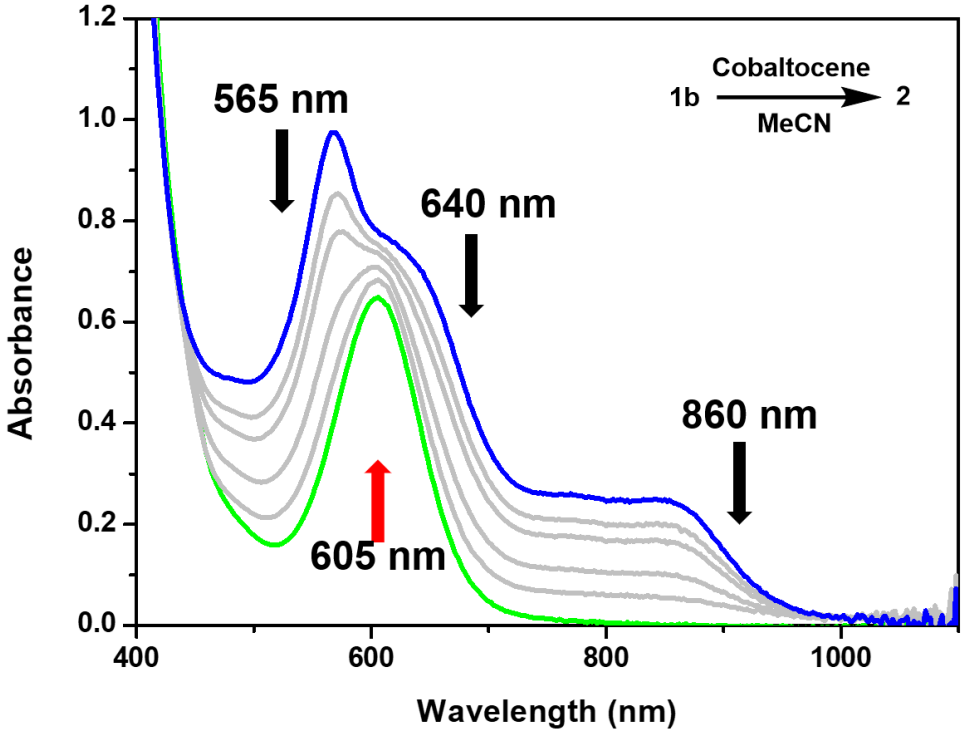

Figure S26. UV-Vis spectral changes upon addition of NaO^{t}Bu (total 1 equivalent; 0.2 equivalent each time) to **1b** in CH_3CN at room temperature.

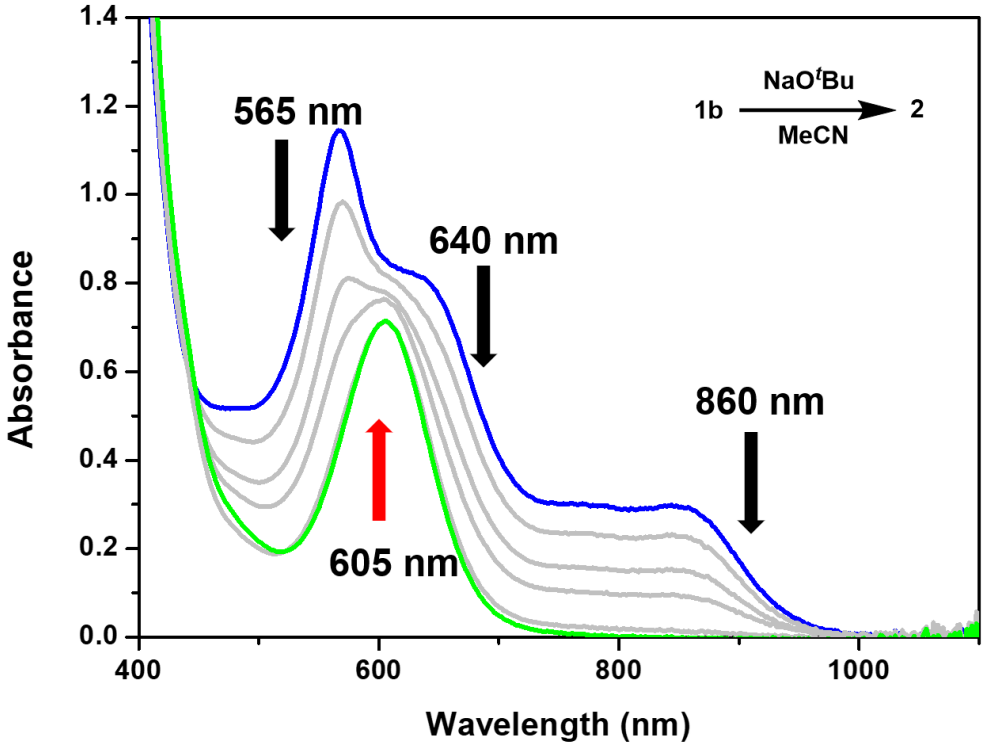

Figure S27. UV-Vis spectral change upon addition of ferrocenium tetrafluoroborate (1 equivalent) to **2** in CH_3CN at room temperature.

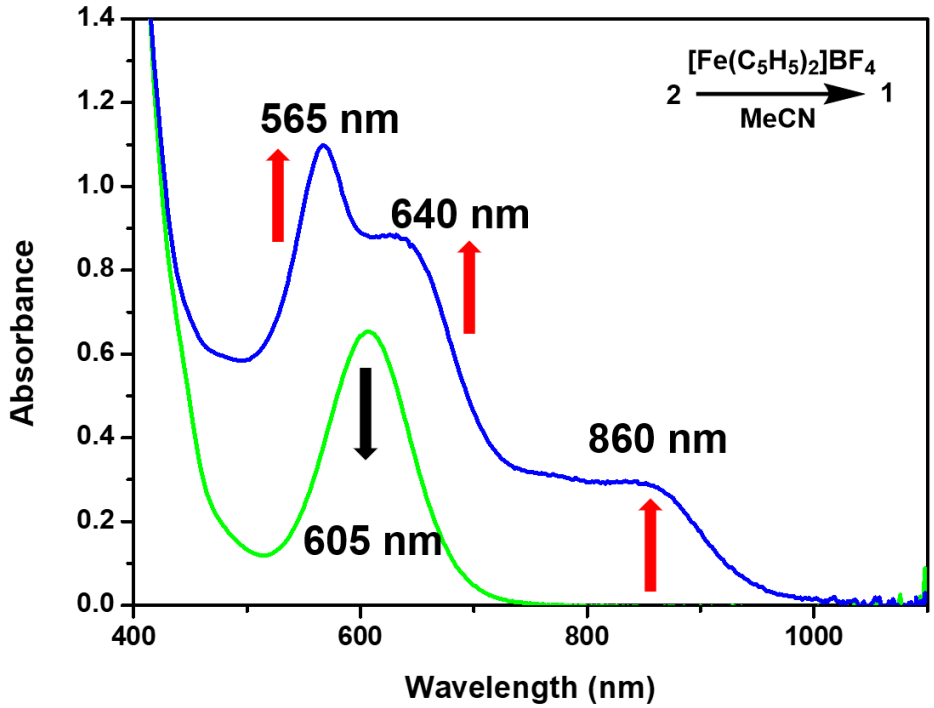

Figure S28. UV-Vis spectral change upon addition of air and $NaPF_6$ to **2** in CH_3CN at room temperature.

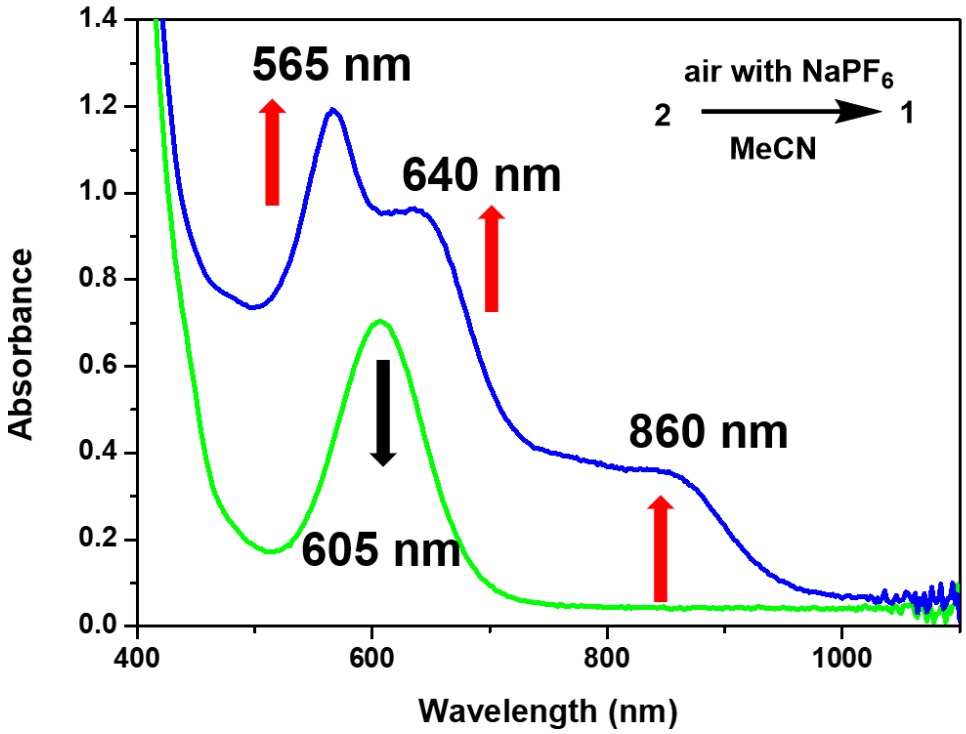

Figure S29. UV-Vis spectral change upon reaction of **2** with air in CH_3CN at room temperature.

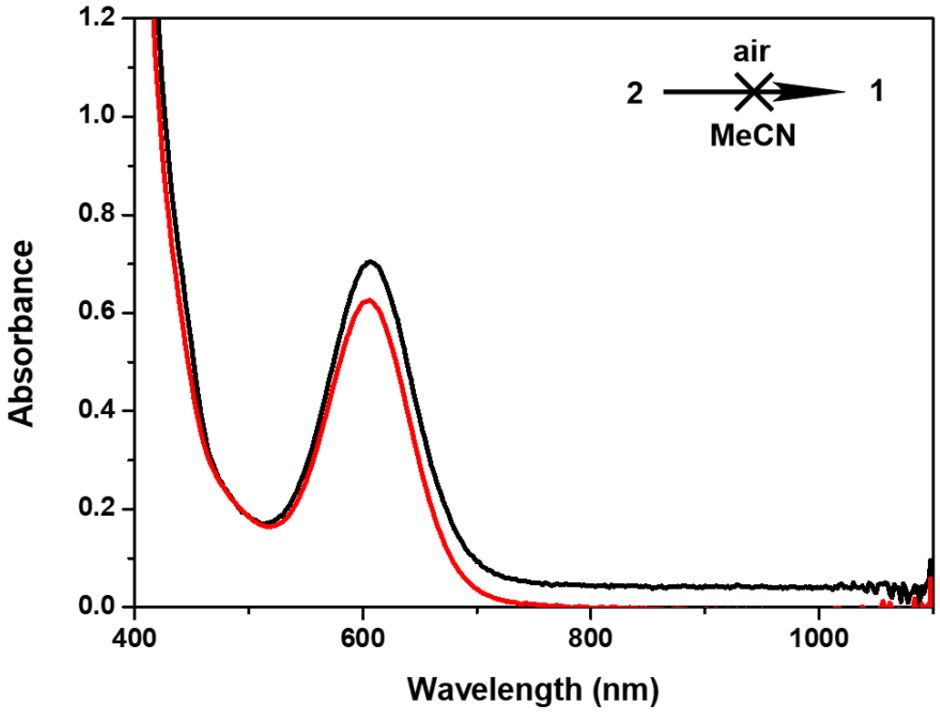

Figure S30. UV-Vis spectral change upon addition of hydrogen peroxide and $NaPF_6$ to **2** in CH_3CN at room temperature.

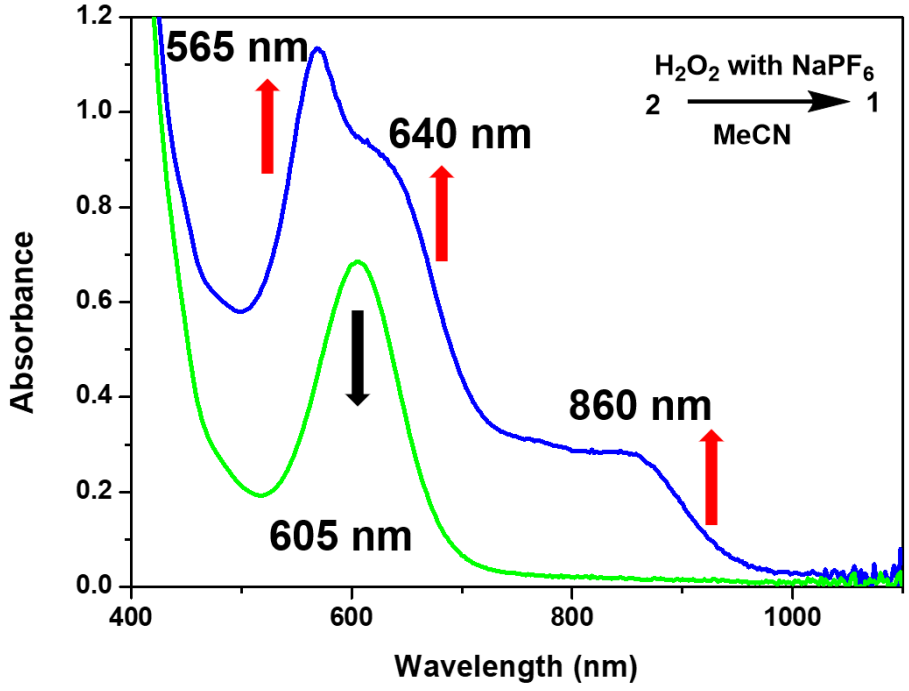

Figure S31. UV-Vis spectral change upon reaction with hydrogen peroxide to **2** in CH_3CN at room temperature.

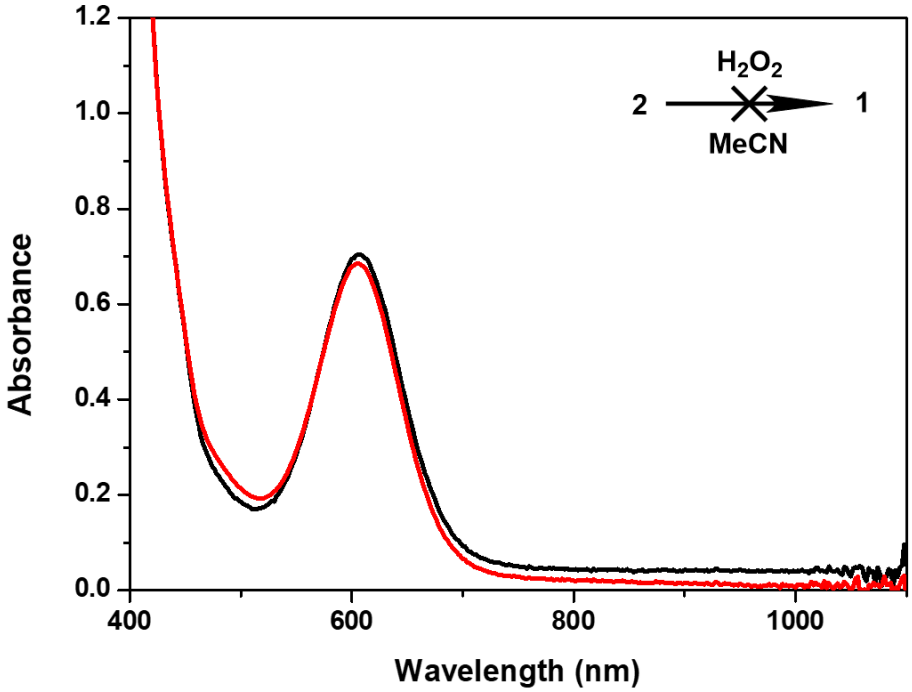

Figure S32. Stability test for **1b** (black spectra) monitored by UV-Vis spectroscopy under air or water conditions at room temperature.

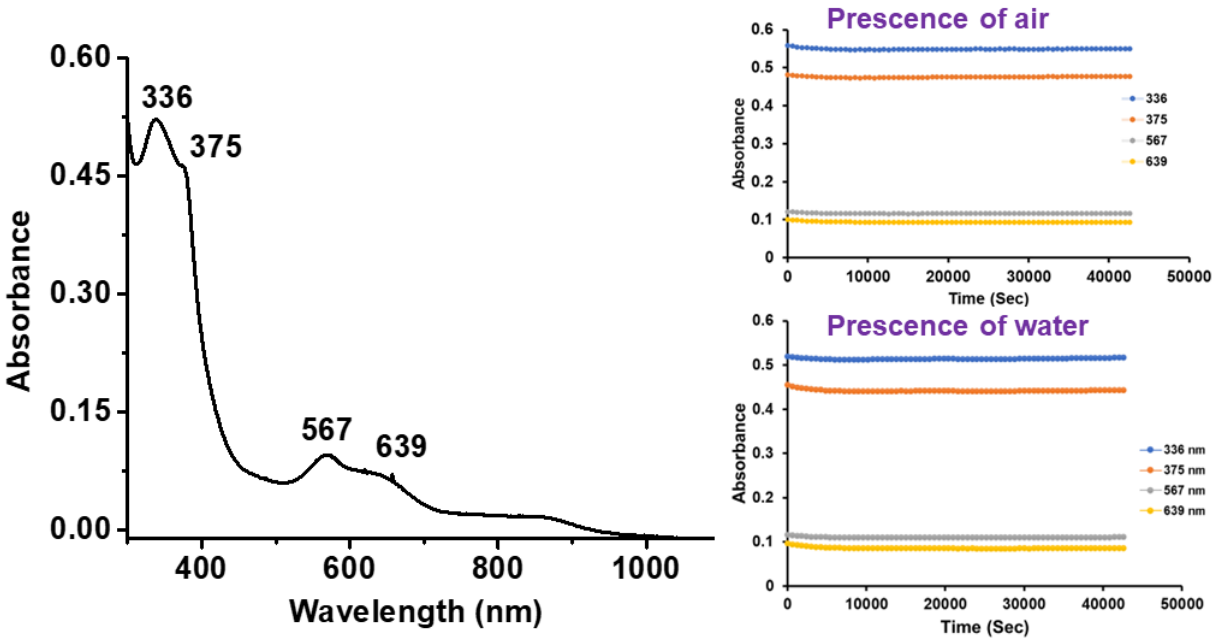

Figure S33. IR spectrum of **A** (KBr pellet).

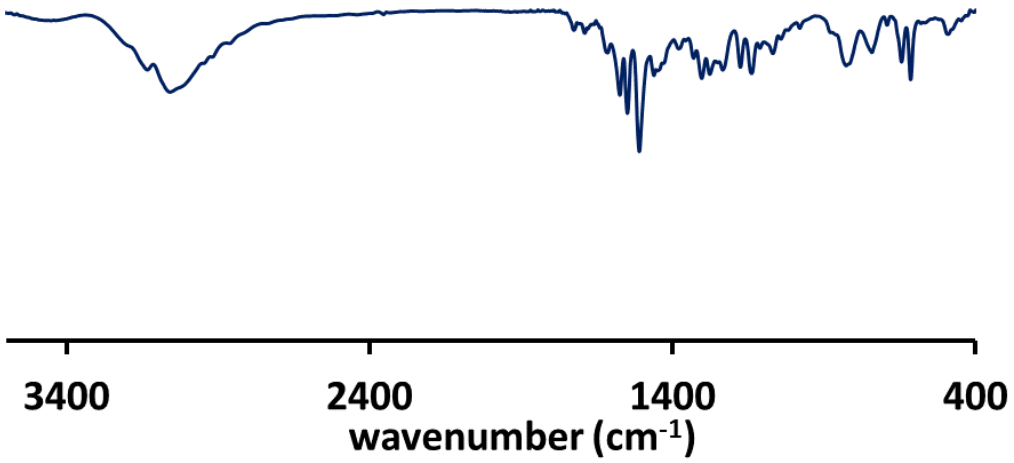

Figure S34. IR spectrum of **B** (KBr pellet).

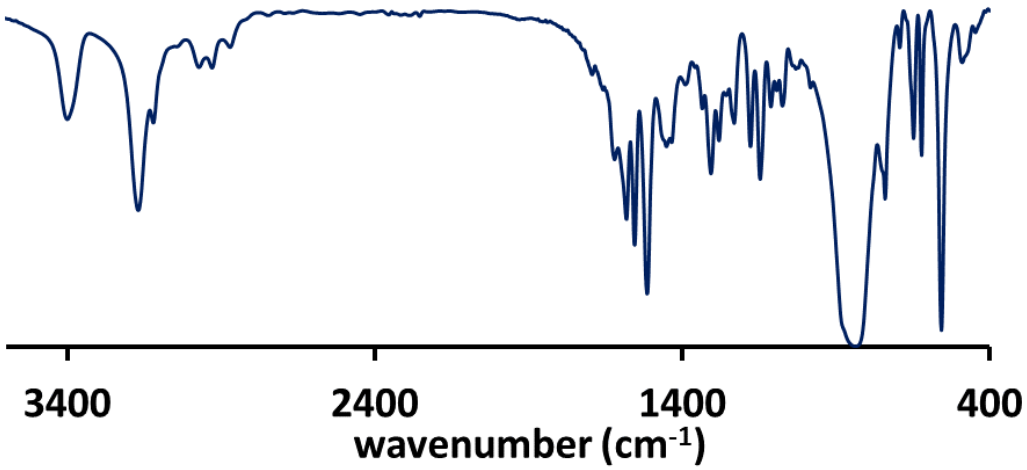

Figure S35. IR spectrum of **1a** (KBr pellet).

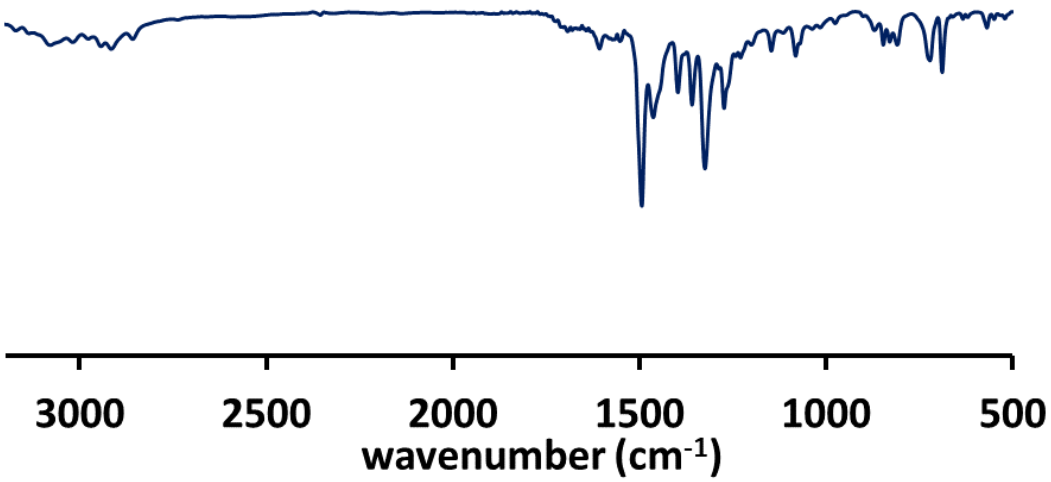

Figure S36. IR spectrum of **1b** (KBr pellet).

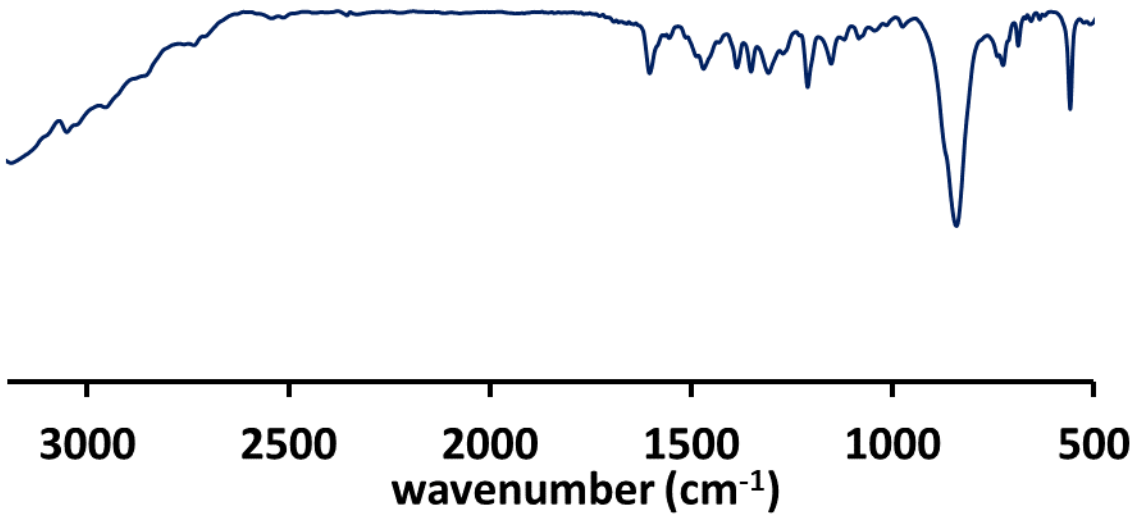

Figure S37. IR spectrum of **2** (KBr pellet).

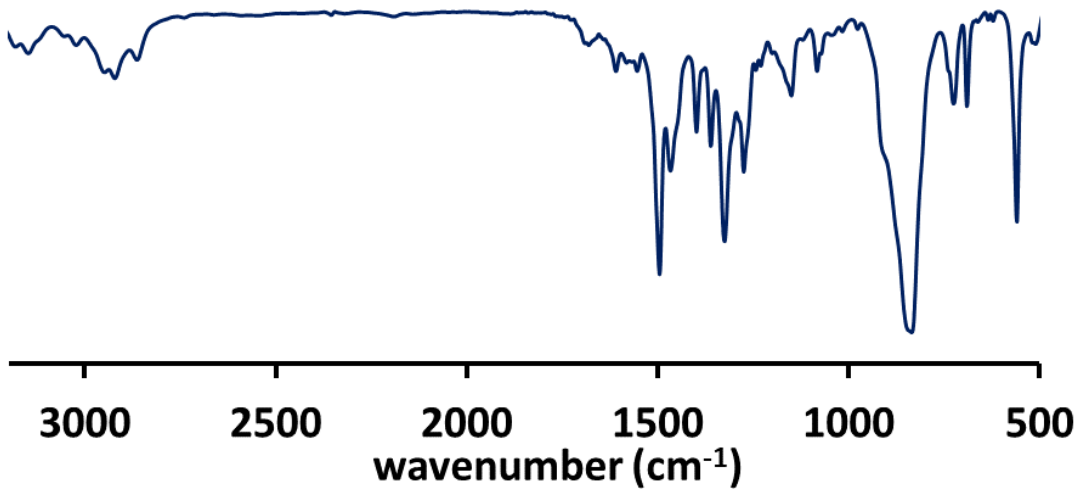

Figure S38. EPR spectrum of **1b** in CH_2Cl_2 collected at room temperature. Simulation parameter g = 2.0153, A_{Co} = 28 G.

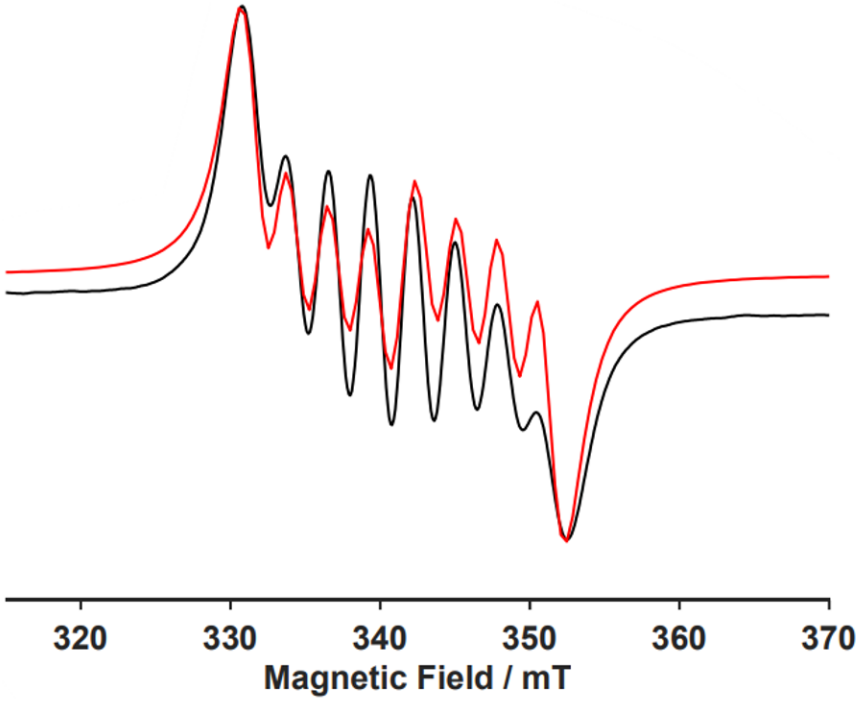

Figure S39. EPR spectrum of **1b** in DMF collected at 20 K. Simulation parameter g = [2.038, 2.009, 1.999], g_{iso} = 2.0153, A_{Co} = [5, 73, 6] G, A_{iso} = 28 G.

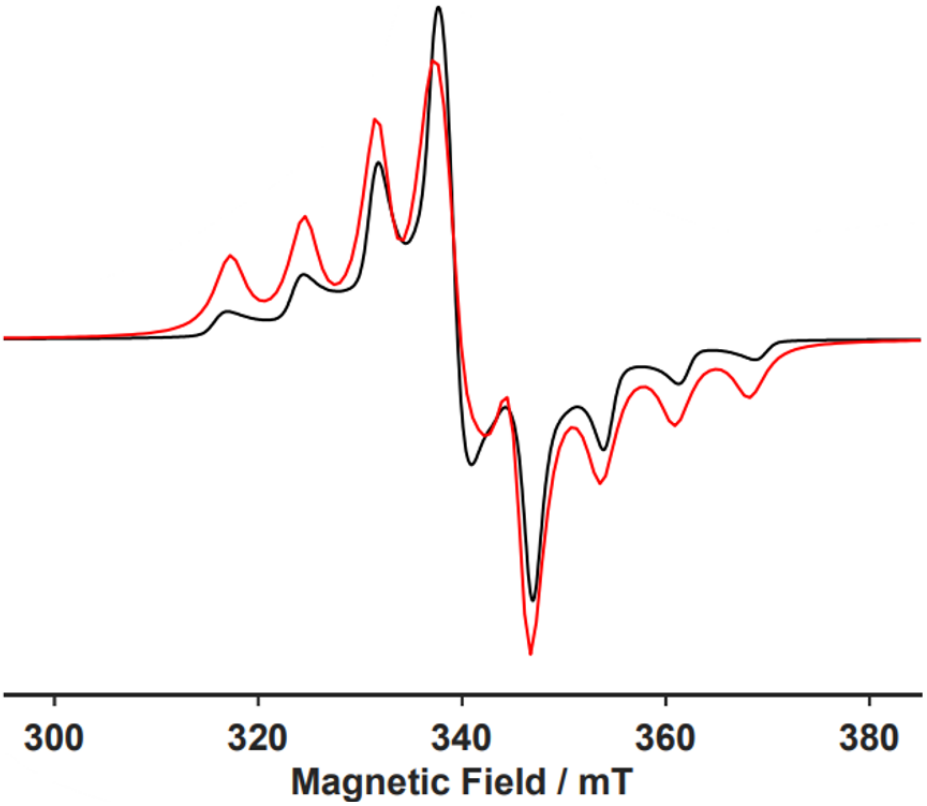

Table S6. Comparison of EPR parameters of selected metal-aminyl complexes.

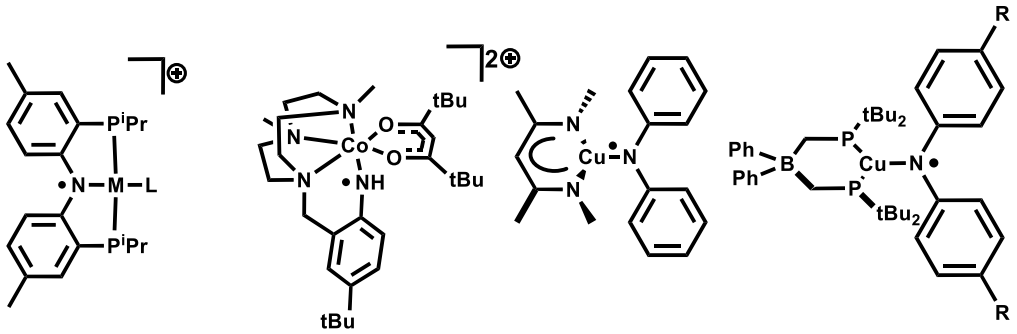

1a-c **2** **3** **4**

M = Ni (a), Mn (b), Re (c)

L = Cl (a), $(CO)_3$ (b,c)

Entry	Simulation Parameter	T	Reference
1a	g_{iso}= 2.0238 A^N_{iso}= 27 MHz A^P_{iso}= 22 MHz A^H_{iso}= 14 MHz, A^H_{iso}= 9 MHz	292 K	J. Am. Chem. Soc. 2008, 130, 3676-3682
1b	g_{iso}= 2.004 A^{Mn}_{iso}= 52 MHz A^N_{iso}= 25 MHz	4 K	Inorg. Chem. 2009, 48, 9214-9221
1c	g_{iso}= 2.013 A^{Re}_{iso}= 169 MHz	4 K	Inorg. Chem. 2009, 48, 9214-9221
2	g_{iso}= 2.0023 A^{Co}_{iso}= 34 MHz A^N_{iso}=24 MHz A^H_{iso} (NH)= 29 MHz A^H_{iso}= 26 MHz (benzylic CH_2)	298 K	J. Am. Chem. Soc. 2000, 122, 9663-9673
3	g_{iso} = 2.069 A^{Cu}_1 = 298 MHz	30K	Angew. Chem. Int. Ed. 2010, 49, 904-907
	g_{iso} = 2.071 A^N_{iso} = 27 MHz (for two N), A^N_{iso} = 14 MHz (for one N) A^{Cu}_{iso} = 103 MHz	RT	
4	g_{iso}= 2.0153 A^{Cu}_{iso}= 79 MHz A^P_{iso} = 156 MHz A^N_{iso} = 49 MHz	77K	J. Am. Chem. Soc. 2009, 131, 3878-3880

Figure S40. Cyclic voltammogram of **1b** measured in THF with 0.3 M [^{n}Bu$_4$N][PF$_6$] as electrolyte at different scan rates: 100, 200, 300, and 400 mV/s. Amide/aminyl radical couple at –0.25 V and Co^{II}/Co^{III} couple at –2.42 V vs. Fc/Fc$^+$.

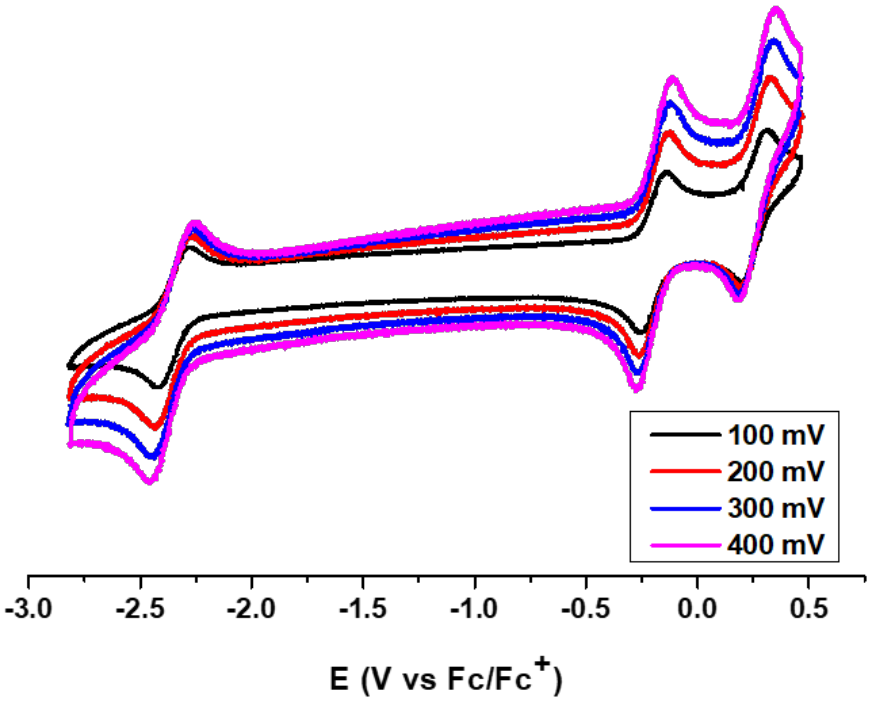

Figure S41. Cyclic voltammogram of **2** measured in THF with 0.3 M [^{n}Bu$_4$N][PF$_6$] as electrolyte at different scan rates: 100, 200, 300, and 400 mV/s. Amide/aminyl radical couple at –0.25 V and Co^{II}/Co^{III} couple at –2.42 V vs. Fc/Fc$^+$.

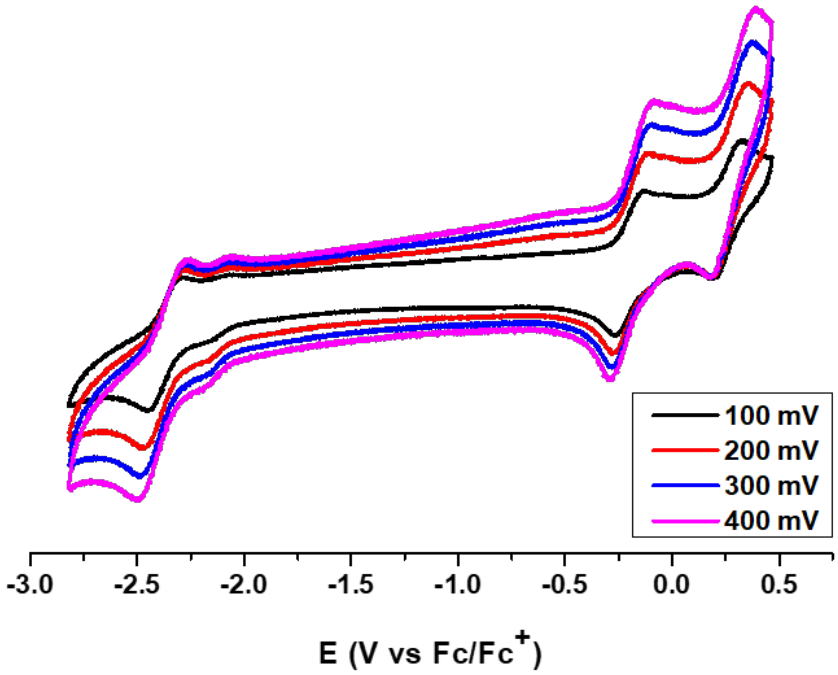

Figure S42. Selected molecular orbitals of **1** (left) and its electronic structure (right) derived from the geometry optimization and frequency calculations using unrestricted B3LYP/Def2-SVP of DFT; energies in cm^{-1}. Lobal representations correspond to orbitals indicated by the number with 0.08 isocontours.

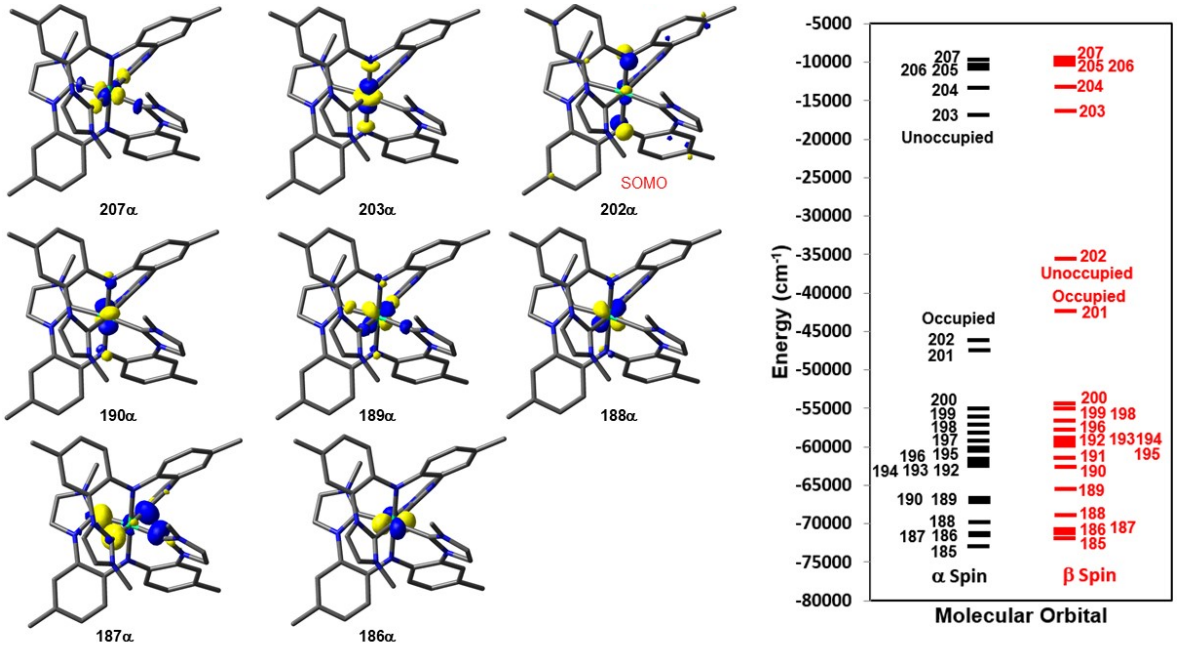

Table S7. Structural parameters of **1** obtained from SC-XRD data and DFT calculations.

		Bond distance (Å)	Bond angles (°)	Wiberg indices
Co–N	Experimental	1.919(4), 1.909(6)		0.5748, 0.5748
	DFT	1.972, 1.972		
Co–C	Experimental	1.949(7), 1.909(6) 1.949(7), 1.951(7)		0.7334, 0.7335 0.7334, 0.7334
	DFT	1.995, 1.995 1.995, 1.995		
∠N–Co–N	Experimental		177.9(3)	
	DFT		180	
∠C–Co–C	Experimental		174.7(3), 175.6(3)	
	DFT		173.2, 173.2	

Figure S43. Calculated molecular orbitals of **1**; alpha spin derived from the geometry optimization and frequency calculations using unrestricted B3LYP/Def2-SVP of DFT. Lobal representations correspond to orbitals indicated by the number with 0.07 isocontours.

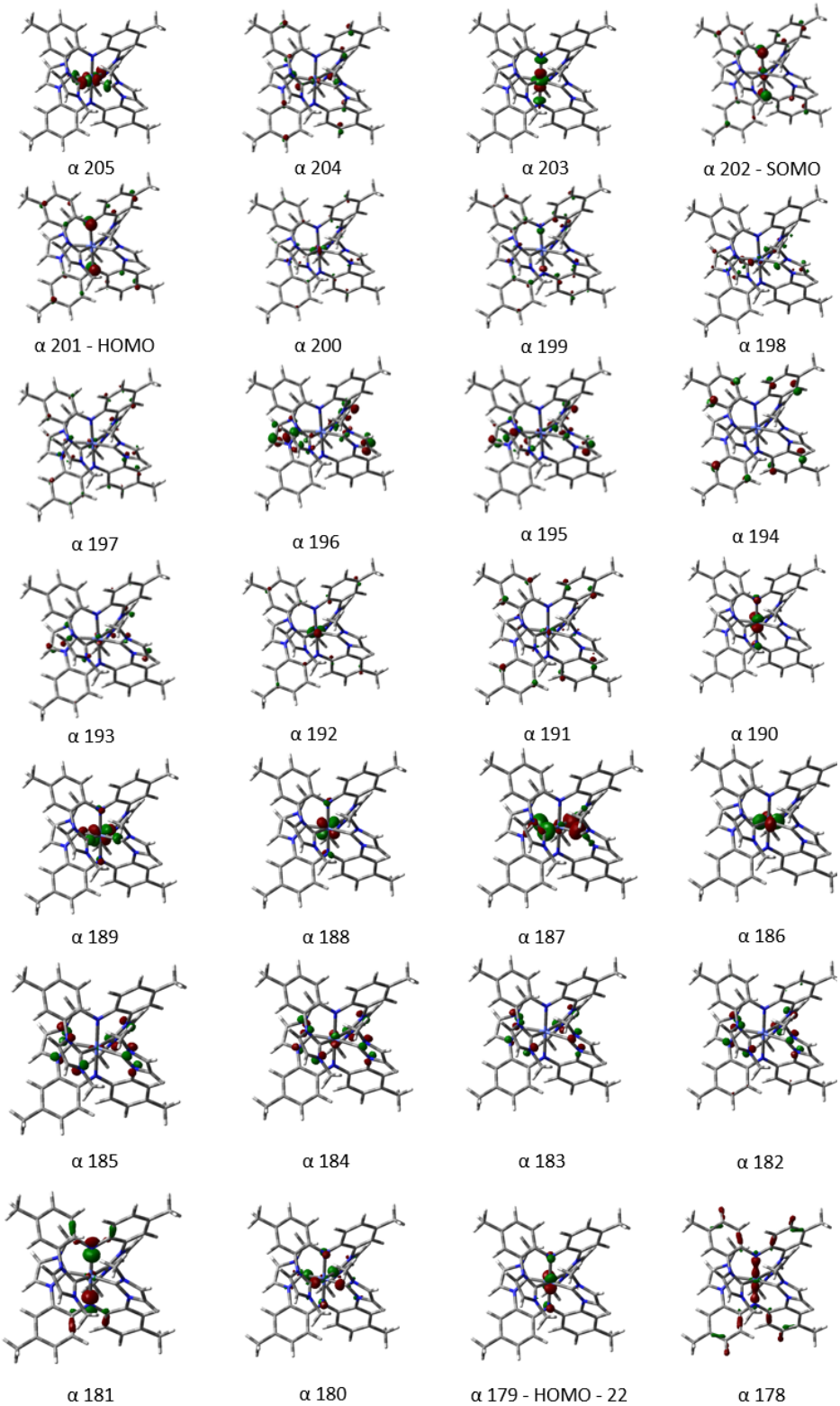

Figure S44. Calculated molecular orbitals of **1**; beta spin derived from the geometry optimization and frequency calculations using unrestricted B3LYP/Def2-SVP of DFT. Lobal representations correspond to orbitals indicated by the number with 0.07 isocontours.

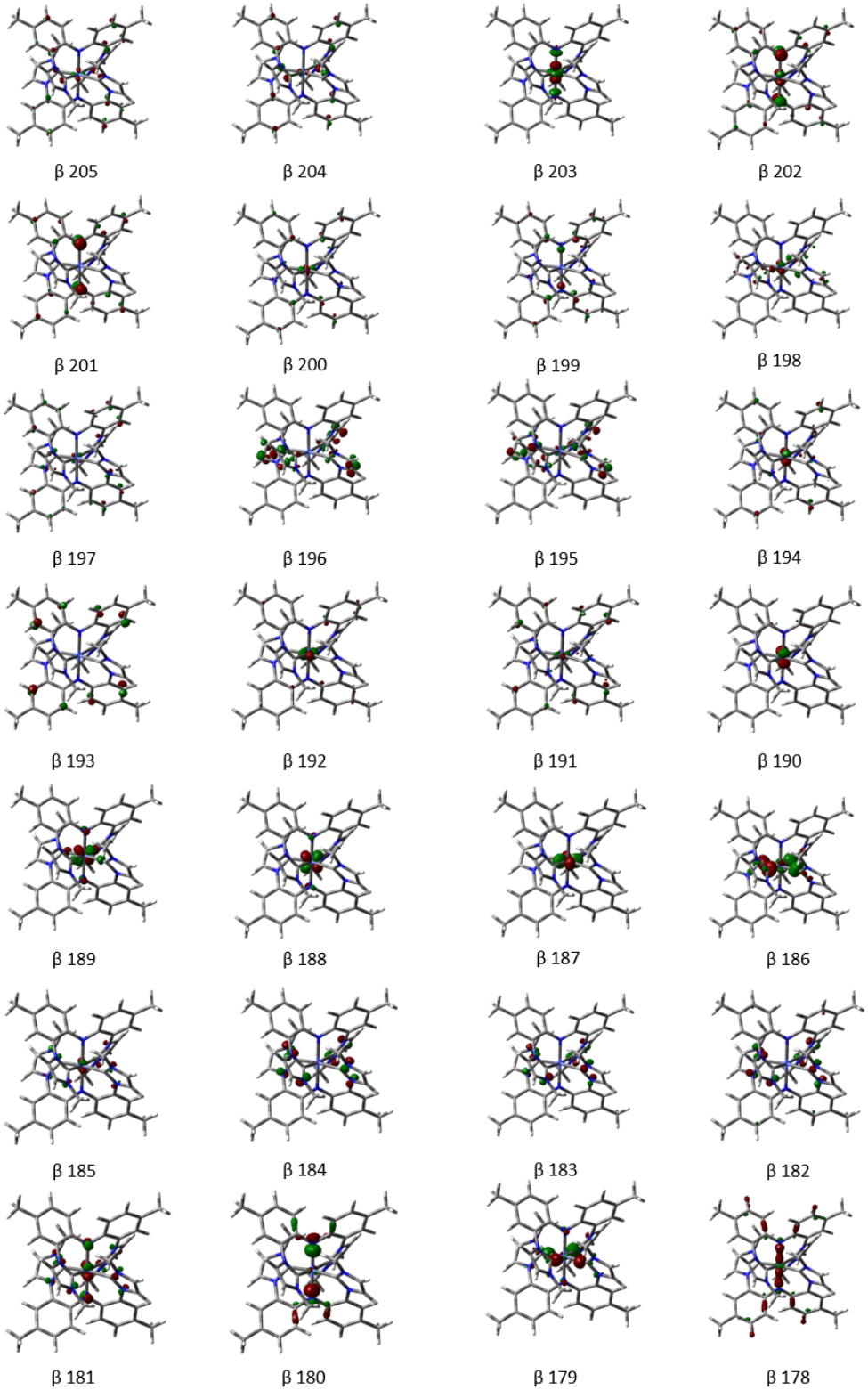

Figure S45. Mulliken spin density plot for **1** obtained by using unrestricted ~~TGVBP~~B3LYP/Def2-TGVBP of DFT. Lobal representations correspond to orbitals indicated by the number with 0.006 isocontours.

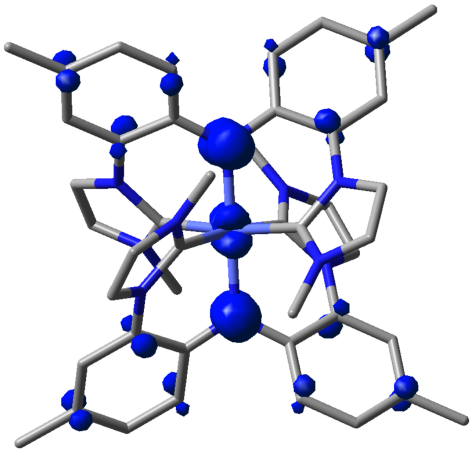

Atom	Spin density
Co	0.107(7)
N1	0.227(7)
N2	0.227(7)

Figure S46. Selected molecular orbitals of **2** (left) and its electronic structure (right) derived from the geometry optimization and frequency calculations using unrestricted B3LYP/Def2-SVP of DFT; energies in cm^{-1}. Lobal representations correspond to orbitals indicated by the number with 0.08 isocontours.

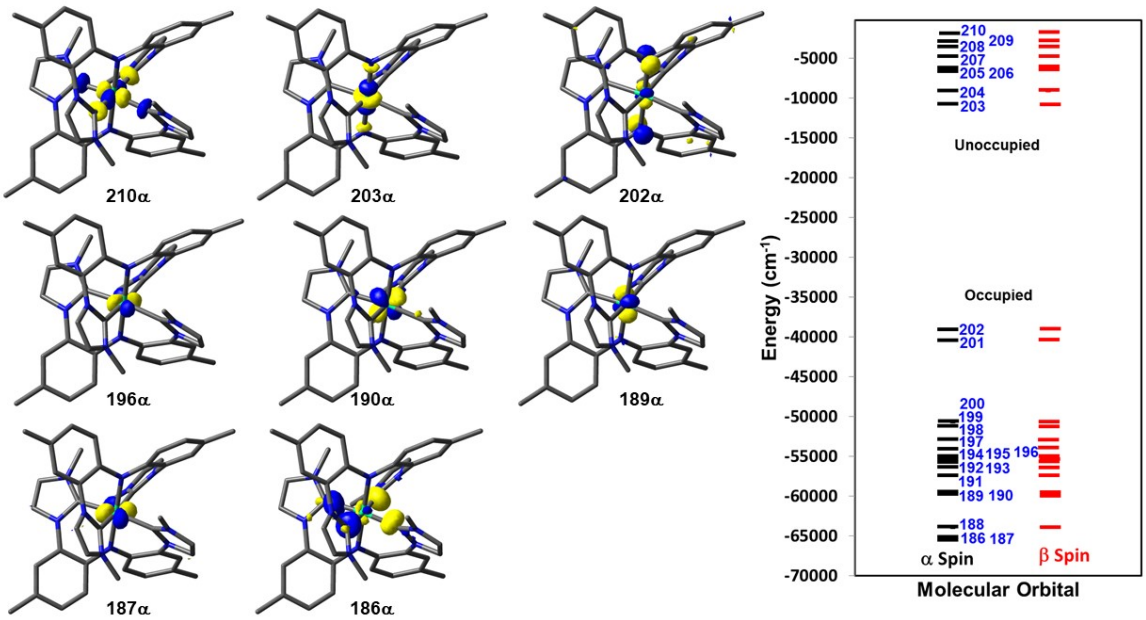

Table S8. The structural parameters for **2** obtained from SC-XRD data and DFT calculations.

		Bond distance (Å)	Bond angles (°)	Wiberg indices
Co–N	Experimental	1.973(5), 1.957(5)		0.5401, 0.5401
	DFT	2.012, 2.012		
Co–C	Experimental	1.930(6), 1.935(7) 1.936(7), 1.939(6)		0.7311, 0.7311 0.7311, 0.7311
	DFT	1.989, 1.989 1.989, 1.989		
∠N–Co–N	Experimental		177.1(2)	
	DFT		180.0	
∠C–Co–C	Experimental		173.7(3), 173.2(3)	
	DFT		172.2, 172.2	

References

1. H. Gilman, E. A. Zuech, *J. Org. Chem*. 1961, **26**, 3481.
2. W. Wang, Y. Qin, M. Luo, P. Xia, M. S. Wong, *Organometallics*. 2008, **27**, 2268.
3. W. Kohn, L. *J. Sham, Phys. Rev*. A. 1965, **140**, 1133.
4. (a) Weigend, *Phys. Chem. Chem. Phys*. 2006, **8**, 1057. 29. (b) F. Weigend, R. Ahlrichs, *Phys. Chem. Chem. Phys*. 2005, **7**, 3297. 30. (c) A. D. Becke, *J. Chem. Phys*. 1993, **98**, 1372. 31.
5. M. Cossi, N. Rega, G. Scalmani, V. Garone, *J. Comput. Chem*. 2003, **24**, 669.